

Gravity at the horizon: on relativistic effects, CMB-LSS correlations and ultra-large scales in Horndeski's theory

Janina Renk^{a,b,c} Miguel Zumalacárregui^{b,a} Francesco Montanari^d

^aInstitut für Theoretische Physik, Ruprecht-Karls-Universität Heidelberg,
Philosophenweg 16, 69120 Heidelberg, Germany

^bNordita

KTH Royal Institute of Technology and Stockholm University
Roslagstullsbacken 23, SE-106 91 Stockholm, Sweden

^cThe Oskar Klein Centre for Cosmoparticle Physics, Stockholm University
AlbaNova University Center, SE-106 91 Stockholm, Sweden

^dPhysics Department, University of Helsinki and Helsinki Institute of Physics,
P.O. Box 64, 00014, University of Helsinki, Finland

E-mail: renk@thphys.uni-heidelberg.de, miguel.zumalacarregui@nordita.org,
francesco.montanari@helsinki.fi

Abstract. Observations of cosmological large scale structures (LSS) offer a unique opportunity to test the nature of gravity. We address the impact of consistent modifications of gravity on the largest observable scales, focusing on relativistic effects in galaxy number counts and the cross-correlation between the matter distribution and the cosmic microwave background temperature anisotropies. Our analysis applies to a very broad class of general scalar-tensor theories encoded in the Horndeski Lagrangian and is fully consistent on linear scales, retaining the full dynamics of the scalar field and not assuming quasi-static evolution. As particular examples we consider both, self-accelerating covariant Galileons and parameterizations of the properties that fully describe the linear theory. We investigate the impact of these models on relativistic corrections to galaxy clustering using the `hi_class` code. We find that especially effects which involve integrals along the line of sight (gravitational lensing, time delay and the integrated Sachs-Wolfe effect, ISW) can be considerably modified, and even lead to $\mathcal{O}(1000\%)$ deviations from General Relativity in the case of the ISW effect for Galileon models, for which standard probes such as the growth function only vary by $\mathcal{O}(10\%)$. These effects become dominant when correlating galaxy number counts at different redshift and can lead to $\sim 50\%$ deviations in the total signal that might be observable by future LSS surveys. To isolate the ISW effect we consider the cross-correlation between LSS and cosmic microwave background temperature anisotropies and use current data to further constrain Horndeski models. Forthcoming large-volume galaxy surveys using multiple-tracers will search for all these effects, opening a new window to probe gravity and cosmic acceleration at the largest scales available in our Universe.

Contents

1	Introduction	1
2	Relativistic effects in galaxy number counts	3
3	Scalar-tensor gravity	7
3.1	Covariant Galileons	9
3.2	Parameterized Horndeski gravity	10
3.3	Covariant Galileons in the parameterized language	11
4	Galaxy number counts and relativistic effects in Horndeski gravity	11
4.1	Covariant Galileons	13
4.2	Parameterized Horndeski gravity	16
4.2.1	Kineticity	17
4.2.2	Tensor Speed Excess	18
4.2.3	Running effective Planck Mass	18
4.2.4	Braiding	21
5	GNC-CMB temperature correlation in Horndeski gravity	22
6	Conclusions	24
A	Transfer functions	27

1 Introduction

The mechanism behind cosmic acceleration is one of the deepest mysteries confronted by modern science and might hold key information for our understanding of fundamental physics. One possibility for such a mechanism is a breakdown of Einstein’s General Relativity (GR) on cosmological scales due to the presence of additional degrees of freedom [1]. Independently of possible connections with the phenomenon of cosmic acceleration, current and forthcoming cosmological observations will allow us to test gravity through many effects predicted by alternative theories using observations of the universe’s expansion and the formation of large scale structure (LSS) [2–4]. The area and depth covered by forthcoming surveys [5–7] will extend this search for anomalous gravitational effects on increasingly larger volumes, eventually reaching into ultra-large scales comparable to the Hubble radius.

The Newtonian description of gravity becomes inaccurate on large cosmological scales, leaving room for relativistic effects that are otherwise negligible [8–10].¹ Gravitational information takes cosmological timescales to travel across such vast distances, making the system’s relaxation time comparable to its characteristic evolution rate. Distortions of the

¹We will follow the convention and refer to relativistic effects as those which are sub-dominant on scales much smaller than the Hubble horizon (see Table 1 and section 2). However, we note that many effects that are often referred to as “Newtonian”, such as redshift-space distortions and gravitational lensing, are also fully relativistic in nature. Similarly, we will adopt the convention of referring to Einstein’s theory of gravity as General Relativity, despite the fact that all the theories we are considering obey the same principles and only distinguish themselves through the presence of additional degrees of freedom.

light-cone caused by gravitational potentials can also affect the observables. This and other effects have to be taken into account, at least in principle, and a growing body of literature is addressing the impact of these effects in LSS observations, as well as devising strategies to detect them with the next generation of galaxy surveys [11–16].

Relativistic corrections to cosmological observables can provide new means to test gravity. Ultra-large scales are interesting not only because these corrections become more important, but offer a number of advantages for cosmological tests of gravity. The largest scales observable today have crossed the Hubble horizon at the onset of cosmic acceleration and are therefore attuned to the energy scale of any additional degree of freedom related to this phenomenon. Such large scales are very well described by linear theory and are the best bet to avoid screening mechanisms that strongly suppress the modifications of gravity due to non-linear effects [17]. These screening mechanisms are predicted in many theories of gravity and can be very efficient in erasing the observational signatures on small and intermediate scales. Finally, relativistic effects have a direct dependence on the metric perturbations and their evolution, which depends critically on the theory of gravity.

One of the fundamental observables in galaxy surveys are the Galaxy Number Counts (GNC’s), which can be studied statistically through n -point correlation functions. Theoretical predictions for GNC’s can incorporate all relativistic effects. GNC’s depend only on directly observable quantities (angles and redshifts of galaxies). Therefore, angle and redshift dependent spectra can be consistently related to observations on arbitrary angular scales and redshift slicings without assuming a fiducial background expansion, thus offering considerable advantages over correlation functions in comoving space. In this sense, GNC angular statistics are the analogue of cosmic microwave background (CMB) spectra, with additional redshift dependence to take into account the 3-dimensional nature of the galaxy distribution. Future surveys such as DESI, Euclid, SKA and the LSST [5–7, 18] are expected to provide competitive measurements of such observables [19].

Combining different observables is also a promising way to constrain gravity. Galaxy and cosmic microwave background cross-correlations probe the late-time evolution of Bardeen potentials through the CMB integrated Sachs-Wolfe (ISW) effect [20–24]. While non-linearities affect correlation functions on small scales, large enough angular scales can be studied using linear theory and provide valuable information about the evolution of Dark Energy. Correlation of CMB data with future large scale surveys are expected to bring substantial improvements in discerning different Dark Energy models [25]. CMB-LSS data has been already used to set constraints on alternative theories of gravity such as $f(R)$ [26, 27] and massive bigravity [28]. It has also been discussed that covariant Galileons predict an anti-correlation between galaxies and the temperature anisotropies in the CMB [29], which is in contradiction to the prediction of Λ -GR and the latest analysis by Ferraro et al. [24] using data from the WISE survey [30].

Addressing the consequences of modified gravity on scales comparable to the Hubble radius requires going beyond the usual approximations valid on small scales. Most studies of LSS formation in alternative theories have been performed under the assumption of quasi-static (QS) evolution, in which the dynamics of the field are neglected [31, 32]. This approximation has been shown to be consistent on small enough linear scales on which the dynamics have relaxed to the equilibrium values, with the regime of validity characterized by the sound horizon of the new degrees of freedom [33]. For this reason, the QS approximation is generally not consistent on ultra-large scales and it is necessary to solve the full system, either from a concrete theory or from an effective formulation such as the effective

field theory of dark energy (EFT-DE) [34–36]. A particularly transparent application of the EFT-DE has been developed in the context of Horndeski’s theory, the most general local, Lorentz-invariant, scalar-tensor theory described by second order equations of motion. This formalism, due to Bellini and Sawicki, employs properties of gravity instead of geometric quantities to parameterize cosmological perturbations in scalar-tensor theories [37] and has been implemented in the `hi_class` code [38].²

In our analysis we investigate the modifications to the galaxy number counts in a very broad class of theories encompassed in the Horndeski Lagrangian. Our analysis comprehends both, the best fit Galileon models of Barreira et al. [29] as an *ab initio* model, as well as the parameterization of Horndeski proposed by Bellini & Sawicki [37] to separately control the background and the different properties that affect the perturbations. We study systematically the dependence of each term contributing to Galaxy Number Counts on the gravity parameters entering our models. We also split all the contributions according to their scale dependence and physical interpretations. Finally, we discuss some of the most remarkable signatures of modified gravity on the galaxy-CMB temperature anisotropy correlation on large angular scales. We use the results for the measurements of the amplitude of the galaxy-CMB correlation from Ferraro et al. [24] to constrain the Bellini-Sawicki parameterization of Horndeski. Our work expands on previous studies of modified gravity on ultra-large scales based on parameterizations of the solutions not relying on a particular theory [39, 40]. This analysis is meant to serve as a general guide for future tests of gravity through galaxy surveys on very large scales.

In [section 2](#) we review the derivation of the full relativistic galaxy number counts and discuss the scale dependence and detection prospects of the several effects. In [section 3](#) we provide a short recap of scalar-tensor theories of gravity, focusing on the models we are using in our analysis: covariant Galileons and the parameterized Horndeski’s theory of gravity. In [section 4](#) we investigate how the change of the matter and metric perturbations of these models influence the GNC’s and the single contributions to it. Finally, in [section 5](#), we use the cross-correlation between CMB temperature anisotropies and large scale structure to constrain the parameter space of the parameterized Horndeski’s theory of gravity. We conclude with summarizing and discussing our results in [section 6](#).

2 Relativistic effects in galaxy number counts

Let us denote by $N(\mathbf{n}, z)$ the total number of galaxies within a given redshift and angular bin, where $-\mathbf{n}$ is the direction of observation (\mathbf{n} being the photon’s propagation direction) and z is the redshift, and by $V(\mathbf{n}, z)$ the volume integrated within the redshift and angular bin. Then $n_g(\mathbf{n}, z) = dN(\mathbf{n}, z)/dz/d\Omega$ and $\nu(\mathbf{n}, z) = dV(\mathbf{n}, z)/dz/d\Omega$ are the number density of galaxies and the volume density, respectively, per redshift z and solid angle Ω . Galaxy number counts are defined as the contrast with respect to the angle averaged value $\langle n_g \rangle(z)$:

$$\Delta(\mathbf{n}, z) = \frac{n_g(\mathbf{n}, z) - \langle n_g \rangle(z)}{\langle n_g \rangle(z)} \quad (2.1)$$

This observable is used to compute correlation functions to be compared to theoretical models. In the context of perturbation theory [41, 42], density fluctuations (and similarly for other perturbations) are usually described as a subtraction between the true galaxy density

²www.hiclass-code.net

$n_g(\mathbf{n}, z)$ defined on the true space-time and its value $\bar{n}_g(\bar{z})$ on a homogeneous and isotropic Friedmann-Lemaître-Robertson-Walker (FLRW) background:

$$\delta_g(\mathbf{n}, z) = \frac{n_g(\mathbf{n}, z) - \bar{n}_g(\bar{z})}{\bar{n}_g(\bar{z})}, \quad (2.2)$$

Note that even though perturbations are defined on the background space-time for simplicity of notation we indicate the dependence on the observed coordinates, as differences are second-order small. Furthermore, spatial averages of perturbations vanish, such that $\bar{n}_g = \langle n_g \rangle$. Let us introduce the galaxy density per comoving volume $\rho_g(\mathbf{n}, z) = n_g(\mathbf{n}, z)/\nu(\mathbf{n}, z)$. In the following we consider linear perturbation theory which allows to write the volume density in terms of its background value plus a perturbation $\nu(\mathbf{n}, z) = \bar{\nu}(z) + \delta\nu(\mathbf{n}, z)$. Following [9], we write eq. (2.1) to linear order as

$$\Delta(\mathbf{n}, z) = \frac{\rho_g(\mathbf{n}, z) - \bar{\rho}_g(z)}{\bar{\rho}_g(z)} + \frac{\delta\nu(\mathbf{n}, z)}{\bar{\nu}(z)}. \quad (2.3)$$

It can be shown that the two terms on the right hand side are separately gauge invariant. Instead, the δ_g perturbation, defined in eq. (2.2) through the fictitious background coordinates, depends on the specific gauge choice. The first term of eq. (2.3) is the subtraction between the full density and its background value both evaluated at the observed redshift. To compute it with perturbation theory, we want to replace this difference with a subtraction between two space-times, where the background density is then evaluated at the background redshift. To do this, we expand the redshift as $z = \bar{z} + \delta z$. The first term on the right hand side of eq. (2.3) can be written in terms of the redshift perturbations δz by Taylor expanding around \bar{z} :

$$\frac{\rho_g(\mathbf{n}, z) - \bar{\rho}_g(z)}{\bar{\rho}_g(z)} = \delta_g(\mathbf{n}, z) - \frac{d\bar{\rho}_g(\bar{z})}{d\bar{z}} \frac{\delta z(\mathbf{n}, z)}{\bar{\rho}_g(\bar{z})}. \quad (2.4)$$

Similarly, we can also expand the direction of observation $\mathbf{n} = \bar{\mathbf{n}} + \delta\mathbf{n}$ appearing in the volume perturbation.

Hence, given the FLRW background evolution, eq. (2.3) is determined in terms of the density perturbation δ_g (well-known from standard perturbation theory, see [41, 42]), the redshift perturbation δz and the volume perturbation $\delta\nu$. These can be computed by solving the geodesic equations as showed, e.g., in [8–10, 43–45]. As the observable $\Delta(\mathbf{n}, z)$ is gauge-invariant, the computation can be carried out in any gauge. We consider the longitudinal Newtonian gauge:

$$ds^2 = a^2 \left[-(1 + 2\Psi) d\tau^2 + (1 - 2\Phi) \gamma_{ij} dx^i dx^j \right], \quad (2.5)$$

where a is the scale factor, Ψ and Φ the Bardeen potentials, and the spatial part of the metric is

$$\gamma_{ij} dx^i dx^j = [dr^2 + r^2 (d\theta^2 + \sin^2 \theta d\varphi^2)]. \quad (2.6)$$

Here and throughout the paper we use natural units in which $c = 1$.

Galaxy number counts $\Delta_{\text{obs}}(\mathbf{n}, z)$ are given by the sum of the following terms

$$\Delta_{\delta}(\mathbf{n}, z) = b(z) \delta_{\text{co}}(r(z)\mathbf{n}, \tau(z)), \quad (2.7)$$

$$\Delta_{\text{rsd}}(\mathbf{n}, z) = \frac{1}{\mathcal{H}(z)} \partial_r(\mathbf{v} \cdot \mathbf{n}), \quad (2.8)$$

$$\Delta_{\kappa}(\mathbf{n}, z) = -\frac{(2 - 5s(z))}{2} \int_0^{r(z)} dr \frac{r(z) - r}{r(z)r} \Delta_2(\Phi + \Psi), \quad (2.9)$$

$$\Delta_{\text{dop}}(\mathbf{n}, z) = \left[\frac{\mathcal{H}'}{\mathcal{H}^2} + \frac{2 - 5s(z)}{r\mathcal{H}} + 5s(z) - f_{\text{evo}}(z) \right] (\mathbf{v} \cdot \mathbf{n}) + [3 - f_{\text{evo}}(z)] \mathcal{H} \Delta^{-1}(\nabla \cdot \mathbf{v}), \quad (2.10)$$

$$\Delta_{\text{lp}}(\mathbf{n}, z) = (5s(z) - 2)\Phi + \Psi + \mathcal{H}^{-1}\Phi' + \left[\frac{\mathcal{H}'}{\mathcal{H}^2} + \frac{2 - 5s}{r\mathcal{H}} + 5s(z) - f_{\text{evo}}(z) \right] \Psi, \quad (2.11)$$

$$\Delta_{\text{td}}(\mathbf{n}, z) = \frac{2 - 5s}{r(z)} \int_0^{r(z)} dr (\Phi + \Psi), \quad (2.12)$$

$$\Delta_{\text{ISW}}(\mathbf{n}, z) = \left[\frac{\mathcal{H}'}{\mathcal{H}^2} + \frac{2 - 5s}{r\mathcal{H}} + 5s(z) - f_{\text{evo}}(z) \right] \int_0^{r(z)} dr (\Phi' + \Psi'). \quad (2.13)$$

Here \mathbf{v} is the velocity perturbation in longitudinal gauge, $\mathcal{H} = aH$ is the conformal Hubble parameter and Δ_2 is the Laplacian on the sphere. The term $\Delta^{-1}(\nabla \cdot \mathbf{v})$ is the velocity potential (in Fourier space it reads $-V(k)/k$ given the k -mode $V(k)$ of the velocity field) coming from the gauge transformation relating the density perturbation in the Newtonian gauge to the one in the synchronous gauge comoving with dark matter δ_{co} . This is the one entering in the Poisson equation [46, 47] and that should then be multiplied by the (linear) bias factor $b(z)$. All quantities not integrated are evaluated at conformal time $\tau(z)$ and at position $r(z)(-\mathbf{n}) = (\tau_0 - \tau(z))(-\mathbf{n})$. A prime indicates a derivative w.r.t. conformal time. We also introduce the magnification bias $s(z)$ and evolution bias $f_{\text{evo}}(z)$ terms. In particular, the latter takes into account deviations from the conservation of the background comoving galaxy number density $a^3 \bar{\rho}_{\text{g}} = \text{const.}$, assumed in the previous equations.

The first three contributions Δ_{δ} (*intrinsic clustering*), Δ_{rsd} (*Kaiser redshift-space distortions*) and $\Delta_{\kappa}(\mathbf{n}, z)$ (*lensing convergence*)³ are proportional to two spatial derivatives of the Bardeen potentials. The velocity terms Δ_{d} (which we call *Doppler* effects) are instead proportional to one spatial derivative of Bardeen potentials, while the remaining terms depend directly on them. We have defined the *integrated Sachs-Wolfe* effect (ISW) by those terms $\Delta_{\text{ISW}}(\mathbf{n}, z)$ proportional to $\int_0^{r(z)} dr (\Phi' + \Psi')$ and the *Shapiro time-delay* by terms $\Delta_{\text{td}}(\mathbf{n}, z)$ proportional to $\int_0^{r(z)} dr (\Phi + \Psi)$. We refer to local contribution depending on the Bardeen potentials and their time derivatives as *local potential* effects $\Delta_{\text{lp}}(\mathbf{n}, z)$. These terms are summarized in Table 1 and further described in Appendix A. In Fourier space, Doppler and potential terms are suppressed by a factor \mathcal{H}/k and $(\mathcal{H}/k)^2$, respectively, compared to the leading terms. Therefore, they are negligible on scales much smaller than the horizon $k \gg \mathcal{H}$, while they are relevant on large scales $k \sim \mathcal{H}$. Furthermore, terms integrated along

³Note that the fully relativistic expression for convergence κ should be obtained by solving the Sachs equation in a perturbed FLRW universe [48], which then involve other terms than gravitational lensing only, but we include them into the definition of the other effects. It is also worth recalling that κ is a gauge-dependent quantity [49] and, as such, not observable by its own in a relativistic context.

	Effect	scaling	z -dep.	bias dep.	Eq.	Notes
Δ_δ	Intrinsic clustering	$(\frac{k}{\mathcal{H}})^2 \delta g_{\mu\nu}$	Local	b	(2.7)	$z_i \approx z_j$
Δ_{rsd}	Kaiser RSD	$(\frac{k}{\mathcal{H}})^2 \delta g_{\mu\nu}$	Local	-	(2.8)	small Δz
Δ_κ	Lensing convergence	$(\frac{k}{\mathcal{H}})^2 \delta g_{\mu\nu}$	Integrated	s	(2.9)	$z_i \neq z_j$
Δ_d	Doppler effects	$(\frac{k}{\mathcal{H}}) \delta g_{\mu\nu}$	Local	s, f_{evo}	(2.10)	multitracers
Δ_{lp}	Local potentials	$\delta g_{\mu\nu}$	Local	s, f_{evo}	(2.11)	multitracers
Δ_{td}	Shapiro time delay	$\delta g_{\mu\nu}$	Integrated	s	(2.12)	multitracers
Δ_{ISW}	Integrated Sachs-Wolfe	$\delta g_{\mu\nu}$	Integrated	s, f_{evo}	(2.13)	multitracers

Table 1: Summary of relativistic effects including their dependence on scale, redshift and bias. For some effects it has been pointed out which configurations and observables are most sensitive. Relativistic effects have been shown to be detectable through multi-tracer observations with future surveys [14, 15], but they have not been addressed independently. Note that the ISW effect can be isolated by considering CMB-LSS cross-correlations, cf. section 5.

the line of sight (lensing convergence, ISW and Shapiro time-delay) are negligible on small and intermediate radial scales where galaxy clustering is dominated by local contributions. However, they can be relevant if ultra-large radial scale correlations are taken into account in the analysis.

We summarize the scale dependence of the different effects in Table 1, which serve as a guide for detection studies. Local terms such as RSD, Doppler terms and local potentials are enhanced when correlations at the same redshift are taken into account, while they decay on large redshift separations, where instead terms integrated along the line-of-sight (lensing, Shapiro time-delay and ISW) are more relevant. Because of the factors (k/\mathcal{H}) suppression previously discussed, only the intrinsic clustering, RSD and lensing effects are relevant for single tracer analysis, while the other terms (especially the dominant Doppler effects) may be detected combining different large-scale structure tracers [14, 15]. Let us also note that a clear detection of these effects, however, also relies on a good modeling of observational effects not treatable in perturbation theory such as magnification and evolution bias, depending on the source luminosity function.

The results discussed so far do not assume Einstein’s equations and are independent of the gravitational theories as long as galaxies follow geodesics

$$\mathbf{n} \cdot \mathbf{v}' + \mathcal{H} \mathbf{n} \cdot \mathbf{v} - \partial_r \Psi = 0. \quad (2.14)$$

This assumption can be violated in certain scalar-tensor theories of gravity [50]. Departures from geodesic motion can be very strong in theories such as chameleons or symmetrons [51, 52], in which unscreened objects fall in the geodesics of (2.5) while the trajectories of screened objects are determined by a different effective metric involving the scalar field.

⁴ However, departures from geodesic motion (2.14) are very suppressed for many scalar-tensor theories of interest. This includes covariant Galileons and other theories featuring

⁴More specifically, unscreened objects follow the geodesics of the Jordan frame metric 2.5, while screened objects follow geodesics of the Einstein frame metric (as they are not sensitive to the modifications of gravity). The Einstein and Jordan frame metric are related by a field dependent rescaling $g_{\mu\nu}^{(E)} = C(\phi)g_{\mu\nu}$, where the conformal factor $C(\phi)$ depends on the theory.

the Vainshtein screening mechanism [53]. In these cases the modified gravity effects enter only through the different relations between the gravitational potentials and the matter distribution, which will be affected by the additional degree of freedom.

Galaxy number counts can be used to estimate two-point statistics. As motivated in [19], angular power spectra are particularly suited to study relativistic effects, as they depend on the directly observable multipoles ℓ 's (encoding the angular dependence) and redshifts. Being the angular spectra computed into redshift shells, we indicate the correlation between the bins at reference redshifts z_i and z_j by $C_\ell(z_i, z_j)$. Furthermore, the transfer functions $\Delta_\ell^{W_i}$ depend in general on a window function $W(z_i)$ encoding, e.g., information about the galaxy distribution and redshift resolution. The power spectrum of the primordial curvature perturbation $\mathcal{R}(\mathbf{k})$ is defined as

$$k^3 \langle \mathcal{R}(\mathbf{k}) \mathcal{R}(\mathbf{k}') \rangle = \delta_D(\mathbf{k} - \mathbf{k}') P_{\mathcal{R}}(k), \quad (2.15)$$

where $\delta_D(\mathbf{k} - \mathbf{k}')$ is the Dirac delta function, and we also introduce the adimensional spectrum⁵ $\mathcal{P}_{\mathcal{R}}(k) = \frac{k^3}{2\pi^2} P_{\mathcal{R}}(k)$. The redshift and angle dependent power spectra are given by:

$$C_\ell(z_i, z_j) = 4\pi \int \frac{dk}{k} \Delta_\ell^{W_i}(k) \Delta_\ell^{W_j}(k) \mathcal{P}_{\mathcal{R}}(k), \quad (2.16)$$

where the transfer functions $\Delta_\ell^{W_i}$ are given in [Appendix A](#).

Single tracer analysis are mostly sensitive to the density, redshift-space distortions and lensing effects [13] (possibly also to Doppler terms given appropriate survey specifications [54]). Promising detection results for the other terms contributing to GNC's have been obtained in the context of multiple-tracer analysis with angular power spectra [14, 15]. These studies relies on the fact that large scale observables depending on a (deterministic) galaxy bias, such as the local primordial non-Gaussianities parameter, can be measured with a strong reduction of cosmic variance [55]. Also, symmetries in the correlation function can be used to isolate relativistic effects [12, 56–58], opening another new window where our theory of gravity can be constrained. We leave a detailed multi-tracer detection study through relativistic effects of deviations from GR based on Horndeski models as a future project.

3 Scalar-tensor gravity

Alternative theories of gravity require the introduction of additional degrees of freedom or other departures from the minimal assumptions that lead to Einstein's theory. A simple scenario is to postulate an additional scalar field that interacts non-minimally with the metric. In this context Horndeski's theory [59] provides a general framework encompassing scalar-tensor theories that are local, Lorentz-invariant and have their dynamics described by second order equations of motion.⁶ It is given by the following action functional

$$S[g_{\mu\nu}, \phi] = \int \sqrt{-g} \sum_{i=2}^5 \mathcal{L}_i, \quad (3.1)$$

⁵Our conventions are consistent with the unitary normalization of Fourier transforms.

⁶This is a sufficient condition to avoid the introduction of additional, ghost degrees of freedom [60], although not a necessary one [61, 62]. Note that theories beyond Horndeski are actually *more restricted* than Horndeski because of the less efficient Vainshtein mechanism [63], the lower effective field theory cutoff [64] and the presence of ghosts when combined with Horndeski terms [65].

where the different pieces can be written as:

$$\mathcal{L}_2 = G_2(X, \phi), \quad (3.2)$$

$$\mathcal{L}_3 = -G_3(X, \phi)\square\phi, \quad (3.3)$$

$$\mathcal{L}_4 = G_4(X, \phi)R + G_{4,X} [(\square\phi)^2 - \phi_{;\mu\nu}\phi^{;\mu\nu}], \quad (3.4)$$

$$\mathcal{L}_5 = G_5(X, \phi)G_{\mu\nu}\phi^{;\mu\nu} - \frac{1}{6}G_{5,X} [(\square\phi)^3 - 3(\square\phi)\phi_{;\mu\nu}\phi^{;\mu\nu} + 2\phi_{;\mu}{}^{;\nu}\phi_{;\nu}{}^{;\lambda}\phi_{;\lambda}{}^{;\mu}]. \quad (3.5)$$

Horndeski's theory has attracted considerable attention as a general framework that encompasses many theories of interest, including Brans-Dicke [66], quintessence, kinetic gravity braiding [67], covariant galileons [68, 69], Gauss-Bonnet couplings [70, 71], disformal gravity [72, 73] and some degravitation models [74, 75].

In order to tame the vast functional freedom of Horndeski's theory, several approaches have been devised to describe the dynamics of linear perturbations over a cosmological background [34, 35, 76]. A particularly clear formulation to capture linear structure formation in these models has been developed by Bellini and Sawicki [37].⁷ In their formalism, the perturbed dynamics are determined by the background contribution Ω_{de} and a set of four dimensionless functions that depend on time and represent distinct physical properties of the theory:

- The *kineticity* α_K characterizes the standard kinetic term for the scalar degree of freedom and modulates the speed of sound for scalar perturbations. It receives contributions from all of the Horndeski functions (except a potential term $G_2(\phi)$) and is the only nonzero α -parameter in models with only G_2 such as quintessence and K-essence. Note that in the limit of quasi-static evolution the dynamics become independent of the kineticity.
- The *braiding* α_B characterizes the non-diagonal part of the kinetic term, i.e. it causes second time derivatives of the gravitational potential to enter the equation of the scalar field and vice-versa. This *kinetic mixing* between the metric and scalar degrees of freedom is a characteristic property of scalar-tensor theories [79]. α_B is sourced by $G_{3,X}$, G_4 and G_5 and is responsible for the scale dependence of the effective gravitational constant.
- The *running* $\alpha_M = \frac{d\log(M_*^2)}{d\log(a)}$, or time variation of the effective Planck mass M_* generalizes the notion of an evolving gravitational constant. A non-zero value of α_M is equivalent to a violation of energy conservation (e.g. in the Einstein frame representation of Brans-Dicke theories). It is sourced by G_4 and G_5 and for generalized Brans-Dicke theories in which $G_4 = f(\phi)$ satisfies $\alpha_M = -\alpha_B$.
- The *tensor speed excess* α_T captures the difference between the speed of light and the propagation speed of tensor modes on a cosmological background $c_{GW} = 1 + \alpha_T$. This phenomenon implies a different causal structure for matter and gravity and induces an offset between the two scalar gravitational potentials. It occurs in theories with $G_{4,X}$ or G_5 .

⁷For extensions to the non-linear regime see [77, 78].

Fixing a background evolution for $H(t)$, the matter density parameter today Ω_m , and the four functions α_i 's fully determines the evolution of large-scale structure providing a minimal set of functions able to describe all models consistent with Horndeski gravity at linear order in perturbation theory. The first two functions (α_K, α_B) characterize the kinetic term for the scalar degree of freedom. Their interplay determines the *braiding scale*

$$\frac{k_B^2}{a^2 H^2} \equiv \frac{\alpha_K + \frac{3}{2}\alpha_B^2}{\alpha_B^2} \left[\left(1 - \frac{\Omega_m}{M_*^2}\right) (1 + w_X) + 2(\alpha_M - \alpha_T) \right] + \frac{9}{2} \frac{\Omega_m}{M_*^2}, \quad (3.6)$$

responsible for the scale-dependent growth predicted by scalar-tensor gravity in the quasi-static regime [31, 32]. The last two functions (α_M, α_T) can be thought of as genuine modifications of gravity, as they enter the evolution equation for tensor modes on a cosmological background and also introduce an offset between the two gravitational potentials [80].

In addition, we require stability of the perturbations on all scales. This amounts to demanding a positive scalar kinetic term $D \equiv \alpha_K + \frac{3}{2}\alpha_B > 0$ and speed of sound

$$c_s^2 = \left[(2 - \alpha_B) [6 + \alpha_B + 2\alpha_M - \alpha_T (2 - \alpha_B) + 3(w_{de}\Omega_{de} + w_m\Omega_m)] - 6(2 + w_m) \frac{\Omega_m}{M_*^2} + \frac{2\dot{\alpha}_B}{H} \right] (3\alpha_B^2 + 2\alpha_K)^{-1} > 0, \quad (3.7)$$

as well as similar conditions for tensor modes $M_*^2 > 0$ and $1 + \alpha_T > 0$. Note that the scalar speed of sound (3.7) also determines the sound horizon, below which the field can be considered to evolve quasi-statically [33].

We will consider both, covariant Galileons, as an example of a self-consistent ab-initio model as well as a parameterization of the α functions that determine the dynamics of cosmological perturbations and can be used to study their effects separately.

3.1 Covariant Galileons

The archetypal example of a modern Horndeski theory is the Covariant Galileon [68] as the extension of the flat space-galileons [81] to curved space-time and second-order equations. It is defined by

$$G_2 = c_1\phi - c_2X, \quad G_3 = \frac{c_3}{M^3}X, \quad G_4 = \frac{M_p^2}{2} - \frac{c_4}{M^6}X^2, \quad G_5 = \frac{3c_5}{M^9}X^2. \quad (3.8)$$

We call *cubic*, *quartic* and *quintic Galileons* those models with Lagrangian given by $\mathcal{L}_2 + \mathcal{L}_3$, $\mathcal{L}_2 + \mathcal{L}_3 + \mathcal{L}_4$ and $\mathcal{L}_2 + \mathcal{L}_3 + \mathcal{L}_4 + \mathcal{L}_5$, respectively, when assuming Equation 3.8. In other words, this corresponds to setting both $c_4 = c_5 = 0$, only $c_5 = 0$ or leaving all the c_i 's different from zero, respectively. We use the normalization of the scalar field to set $c_2 = 1$ and will not consider the linear potential $c_1 = 0$ (see Ref. [29] for further details).

The observational viability of this theory has been discussed in ref. [29] (see also [82, 83]), which also provides an excellent introduction into the dynamics of the model. The Covariant Galileon is able to fit the background expansion of the universe and the CMB spectra. However, these models predict a fairly large growth of matter perturbations due to both, the enhanced gravitational force and the larger value of H_0 needed to fit the background expansion [84]. Including neutrino masses alleviates these effects and gives a better fit to data [29].

Note that Galileons are equipped with the Vainshtein screening mechanism, which hides the modifications of gravity on small scales due to the non-linear derivative self-interactions of the scalar degree of freedom. Numerical simulations indicate that the screening becomes effective on sub-horizon scales for the Galileon models we will consider [85, 86]. However, this effect provides an additional motivation to consider ultra-large cosmological scales, in which the linear behaviour is an excellent approximation and no screening mechanisms are active.

3.2 Parameterized Horndeski gravity

It is also possible to consider modifications of gravity not based on any specific Lagrangian by specifying a parameterization of the background expansion and the α -functions. This approach is complementary to the study of specific models, as it allows one to control the different properties of gravity and the cosmological expansion independently. We will adopt the parameterization proposed by Bellini and Sawicki [37]

$$\alpha_i(a) = c_i \Omega_{\text{de}}(a) = c_i \frac{\rho_{\text{de}}}{\rho_{\text{crit}}}, \quad (3.9)$$

the initial effective Planck mass M_* is set to one in units of M_p . The α_i 's and c_i 's correspond to kineticity (α_K and c_K), braiding (α_B and c_B), running Planck mass (α_M and c_M) and tensor speed excess (α_T and c_T), respectively. General Relativity is recovered if all α_i 's are equal to zero. The proportionality of the α_i 's to the energy density of dark energy ensures that we do not include early time modifications to the theory of gravity. Therefore high redshift phenomena, like the CMB, are not altered. The parameterization chosen for the α -functions coincides exactly with simple models such as Kinetic Gravity Braiding [67]. In general it will not reproduce exactly all specific models (see subsection 3.3 for a comparison with Galileons), but it has the advantage of providing in principle a consistent description of the Horndeski Lagrangian, extending other schemes usually adopted, such as parameterizations of the effective gravitational constant and the value of $\Psi - \Phi$ based on the quasi-static approximation (e.g. [40]).

To fully describe the evolution of large-scale structure, besides the α functions (characterizing the perturbations) we need to specify a background evolution. We will assume that the evolution of the scale factor is given by the standard Friedmann equation $H^2 = \frac{8\pi G}{3} (\rho_m + \rho_{\text{de}})$ sourced by matter and a dark energy component with

$$\rho_{\text{de}}(a) = \rho_{\text{de},0} a^{3(1+w)}, \quad (3.10)$$

This background expansion reproduces the results of standard gravity with a cosmological constant (if $w = -1$), therefore allowing us to focus on the novel effects at the level of linear perturbations.

The impact of this model in LSS observables has been addressed in [77], including constraints on the c_i functions using current data [87]. In order to study the effects of each α -function separately we run a series of Markov Chain Monte Carlo analyses varying one or two c_i 's only (see subsection 4.2). Demanding stability of the perturbations on all scales (3.7) is very constraining on these models.⁸

⁸However, if $|c_s^2| \ll 1$ the instabilities will only occur on non-linear scales on which our formalism does not apply. This should hold true for models with the Vainshtein screening, for which standard gravity should be recovered on small scales. The Vainshtein mechanism has been argued to prevent instabilities [88] that are ubiquitous in gravity theories [89].

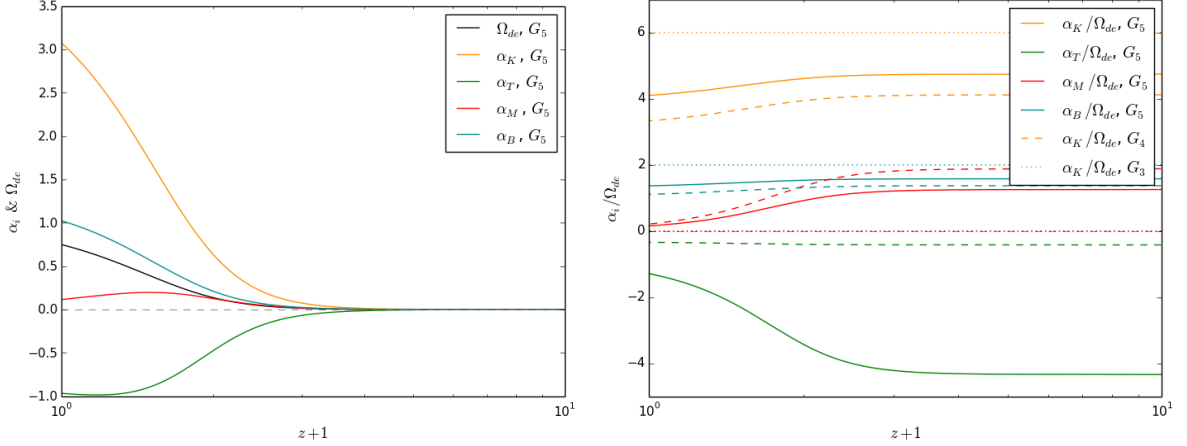


Figure 1: *Left panel:* Ω_{de} and the α -functions for quintic Galileons as a function of redshift. *Right panel:* The value of the ratio α_i/Ω_{de} for cubic, quartic and quintic Galileons over the redshift. Solid, dashed and dotted lines refer to quintic, quartic and cubic Galileons, respectively. Different colors show the evolution of each alpha function characterizing linear perturbations. The model of the parameterization in which α_i is proportional to Ω_{de} can reproduce well those Galileons models with nearly constant ratio α_i/Ω_{de} . Note that cubic Galileons with massive neutrinos show the same behaviour as cubic Galileons without massive neutrinos.

3.3 Covariant Galileons in the parameterized language

To see if the parameterized models we use can reproduce self consistent gravity models, we test if they can approximate the covariant Galileons. The four α -functions for the different Galileon models are plotted in the *left panel* of [Figure 1](#). In the parameterization models we consider we have fixed the α_i 's to be directly proportional to Ω_{de} and we only vary the proportionality coefficients c_i . Therefore the restriction to this models is good if the ratio α_i/Ω_{de} is approximately constant in time for Galileons. This ratio is shown in the *right panel* of [Figure 1](#). The parameterization $\alpha_B = c_B\Omega_{de}$ is exact for cubic, shift-symmetric theories in the attractor. We have checked the qualitative behaviour of the perturbations, the GNC's and their modifications with respect to Λ -GR for cubic Galileons and they are perfectly consistent, despite the different evolution of the equation of state of Galileons.

4 Galaxy number counts and relativistic effects in Horndeski gravity

Let us now analyse how modifications of gravity in the framework of Horndeski theories modify the galaxy number count power spectrum, including all relativistic effects. As an example for fully self consistent gravity models we consider covariant Galileons, more precisely cubic Galileons with and without massive neutrinos as well as quartic and quintic Galileons. After that we investigate how the different α -functions of the effective field theory formulation of Horndeski's gravity affect the galaxy number counts. For each model we analyse how the spectrum of same and different redshift bin correlations are changed w.r.t. a standard General Relativity (GR) model including a cosmological constant, Λ -GR, and to what extent each of the relativistic corrections contributes to this difference. By looking into the growth of perturbations in the different models and how they are related to the relativistic effects we

describe the origin of these deviations and their relation to the properties of gravity. To complete the picture we link the Galileon models to the parameterization formulation and see if the results from the two different approaches are in accordance.

In the following we consider for the Galileon models the best fit background values from Barreira et al. [90]. For the massive neutrinos in cubic Galileons the masses are given by $\Omega_\nu h^2 = 3 \times 0.193 \cdot 10^{-2}$ (degenerate mass for the three families) [90]. For all parameterized Horndeski models we use cosmological parameters consistent with Planck [91]. The power spectra are considered within tophat redshift bins of width $\Delta z = 0.05$, which represents an intermediate configuration between those typically reachable by photometric and spectroscopic redshift determinations. To test cosmological scales both in the early and late dark energy era we consider the redshift bins $z = 0.3$ and $z = 2.5$ as well as the intermediate bin $z = 1$. We set the galaxy bias b to one, neglect magnification and evolution biases, $s = f_{\text{evo}} = 0$, and assume a flat galaxy distribution. All these effects would be relevant for a consistent detection analysis but do not affect our comparison of gravity models.

Before discussing our results for modified gravity theories we will give a brief summary of the most important characteristics of the galaxy number count power spectrum for Λ -GR. We show the total Galaxy Number Counts in Figure 2 for same (*left panel*) and different (*right panel*) redshift bin correlations. Each line corresponds to the contribution of an effect and its cross-correlation with density, including in sequence the dominant terms. E.g., the purple line and shaded region represent the ISW contribution. The blue line from the time-delay corresponds to the sum of time-delay and ISW while the blue area indicates the contribution of the time-delay to it. In the case where only one redshift bin is considered the total GNC's are dominated by the intrinsic density fluctuations and RSD. The lensing magnification and its cross-correlation with the density play a minor role on ultra-large scales but can, depending on the configuration, overcome the RSD on smaller scales (e.g. $\ell \gtrsim 120$ for $z_i = z_j = 0.3$). Further contributions, namely Doppler effects, local potential terms, Shapiro time-delay and the ISW effect, are sub-dominant. For more details see [9].

In the correlation of two different redshift bins (*right panel* of Figure 2) the importance of the local effects decreases with further separation of the bins. The signal is dominated by the negative cross-correlation of lensing magnification and the local effects [13]. The pure lensing contribution is the second largest effect followed by the Shapiro time-delay and ISW effect if considered together with their cross-correlation with the density fluctuations. For redshift bins which are closer together or overlap, local contributions can become important on ultra-large scales and if all their cross-correlations among each other are considered can add up to contribute about 20% to the total signal for $\ell \lesssim 5$.

In addition, we have found that the cross-correlations between the lensing magnification and the integrated relativistic effects, ISW and Shapiro time-delay, are also important to take into account on ultra large scales in the correlation of high, well separated redshift bins. In the configuration $z_i = 1$, $z_j = 2.5$ this contribution is as high as 45% of the total signal at $\ell = 2$. The impact of this contributions and where they can dominate the signal has been studied by Raccanelli et al. [92] Another interesting feature of this redshift bin configuration is that there can be a change of sign in the signal. This happens when the positive lensing magnification is larger than the negative cross-correlation between the local and lensing terms on ultra-large scales. For Λ -GR this is the case for ℓ up to 10. On the scale where the two major effects cancel each other out the signal is dominated by the Shapiro time-delay. This is shown in the right panel of Figure 2. We stress that in practice the sign of the correlation will also depend on observational factors, such as the value of the magnification bias term

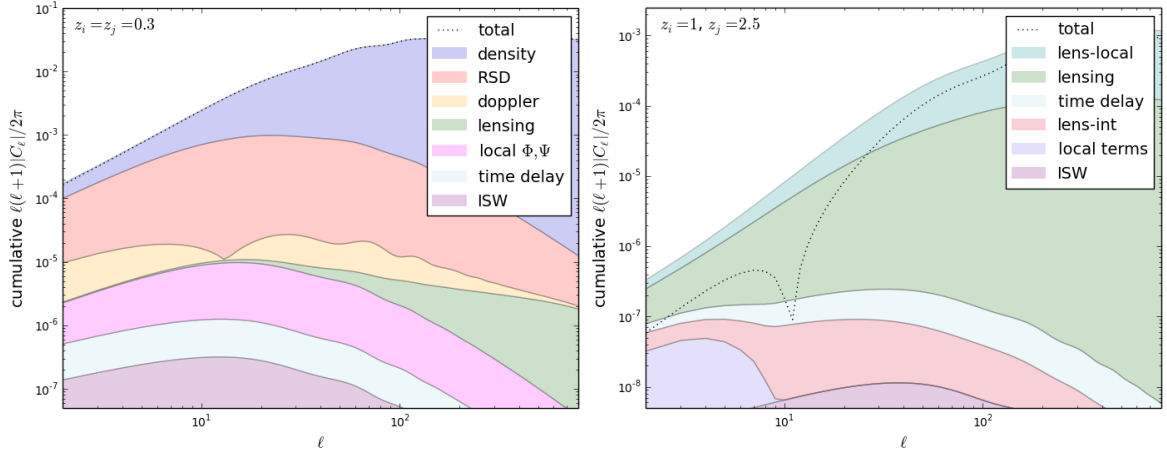


Figure 2: Galaxy number count angular power spectrum for Λ -GR where the coloured regions indicate the contribution of each relativistic effect (2.7-2.13) to the total signal at $z_i = z_j = 0.3$ (left) and $z_i = 1, z_j = 2.5$ (right). Each line corresponds to the contribution of an effect and its cross-correlation with density, including in sequence the dominant terms as explained in the text. We used a tophat window function with bin width $\Delta = 0.05$. Note that the total signal in different bin correlations (right panel) is negative for $\ell \gtrsim 10$, as the dominant local-lensing cross-correlation is negative. The lensing contribution is positive, therefore the total signal is smaller than the sum of the parts in absolute value.

$2 - 5s(z)$ entering in eq. (2.9).

4.1 Covariant Galileons

To understand the modifications to the GNC's we first analyse matter and metric perturbations in the different Galileon models. We use the best fit models for cubic (with and without massive neutrinos), quartic and quintic Galileons from Barreira et al. [29].

All models predict a larger growth of matter perturbations, as already discussed in 3.1. Furthermore the Bardeen potentials are subject to scale depended modifications, which has already been addressed by [29]. Cubic Galileon models do not incorporate anisotropic stress, therefore both Bardeen potentials are changed in the same manner. For modes close to the horizon the modifications are minor while on sub horizon scales the potentials increase after matter domination, instead of a decrease as in Λ -GR. In quartic Galileons the potentials grow as well in the dark energy dominated era for sub horizon modes but the evolution is very flat compared to Λ -GR. Φ can even stay almost constant for modes $k \gtrsim 100\mathcal{H}_0$ while Ψ increases up to a turning point and slowly decreases afterwards. For quintic Galileons the potential increase monotonically in the dark energy dominated era for sub-horizon modes while they decrease in Λ -GR. The deviation w.r.t. Λ -GR on sub horizon scales gradually decrease for increasingly larger k . The modification in the case of cubic Galileons is larger as the extra terms in quartic and quintic models reduce the influence of the fifth force which leads to a less rapid modifications of the evolution of the Bardeen potentials with respect to the cubic case [29].

The enhanced growth of the Bardeen potentials and matter perturbations lead to an increase of the intrinsic density fluctuations, the velocity terms and all contributions which directly depend on the potentials. The total GNC's can be enhanced up to 40% w.r.t. Λ -GR

on ultra large scales. We recall that we fix the amplitude of the CMB fluctuations, already well constrained [3]. We show the total GNC's and all relativistic contributions to it in [Figure 3](#) for Λ -GR, cubic, G_3 , cubic neutrino, νG_3 , and quartic Galileons, G_4 , for $z = 0.3$. Each effect and its cross-correlation with density is shown in the *upper left panel*. The *lower left panel* shows the fractional deviation of each effect w.r.t. the total GNC's of Λ -GR, computed as

$$\frac{C_\ell^{eff.} - C_\ell^{eff., \Lambda-GR}}{C_\ell^{\Lambda-GR}}, \quad (4.1)$$

where at the numerator only the contribution from a single effect (but including its correlations with the density) is considered, while at the denominator we consider the total spectra with all contributions. To see how the single effects are changed more clearly, we plot only the pure effects and their fractional deviation w.r.t. the corresponding effect in Λ -GR in the *right panels*. The oscillations which are visible in the plots for scales $\ell \gtrsim 30$ are due to the misalignment of BAOs caused by the different expansion histories. Indeed, given the BAOs scale $r_{\text{BAO}} \approx 110 \text{ Mpc}/h$, we expect $\ell_{\text{BAO}} = d(z) \frac{2\pi}{r_{\text{BAO}}} \approx 50$ with the comoving distance $d(z)$ at $z = 0.3$.

We find that the integrated effects are the ones which are most sensitive to the changes of gravity in the considered models. For the lensing magnification and the Shapiro time-delay the enhancement w.r.t. Λ -GR is of order 100%, and it can be up to 2000% for the ISW effect. Note that it has a different sign in Galileon models caused by the changed slope of the Bardeen potentials in comparison to Λ -GR. While the negative sign of the ISW in Galileons is not visible in the auto correlation $\langle \Delta_{ISW} \Delta_{ISW} \rangle$ (right panel of [Figure 3](#), it becomes relevant in the cross-correlation with density, $\langle \Delta_\delta \Delta_{ISW} \rangle$. Therefore the contribution from the ISW including its cross-correlation with density is negative in contrast to Λ -GR (note that we plot absolute values in the upper left panel of [Figure 3](#)). This signature will be further discussed in [section 5](#).

Even though the changes in the ISW can be very large, it is the least dominant contributions to the total GNC's and will therefore be hard to detect even in the most optimistic cases. A summary of our results is given in [Table 2](#). It shows the contribution of each effect to the deviation of the $C_\ell(z_i, z_i)$'s with respect to Λ -GR for the fixed scale $\ell = 10$ for the redshift bins $z_i = 0.3, 1$ and 2.5 , and we also include the quintic Galileons G_5 case, which we have omitted from [Figure 3](#) for the purpose of clearness. The effects show a similar scale dependence as in quartic Galileons. The modifications to local terms are less drastic while the terms integrated along the line of sight are increased as the metric perturbation in the quintic case are more enhanced.

In configurations with two different redshift bins the changes are more drastic as the dominating contributions depend on the lensing magnification. Due to the enhancement of the lensing potential in Galileon models the total signal is increased of order 50% even on scales up to $\ell \sim 100$. [Figure 4](#) shows the GNC's and the most important contributions for two different redshift bin configurations. Looking at the *right panel* of [Figure 4](#) the scale on which the total signal changes its sign for $z_i = 1, z_j = 2.5$ is shifted towards smaller scales (larger ℓ) for all Galileon models. This is due to the fact that local terms are not increased as dramatically as integrated terms and hence the scale on which they cancel out is decreased. It is also interesting to notice that in Galileon models the cross-correlation between lensing magnification and the integrated relativistic effects can become larger than the total GNC's in Λ -GR on ultra-large scales. The fractional deviations to Λ -GR for different redshift bin

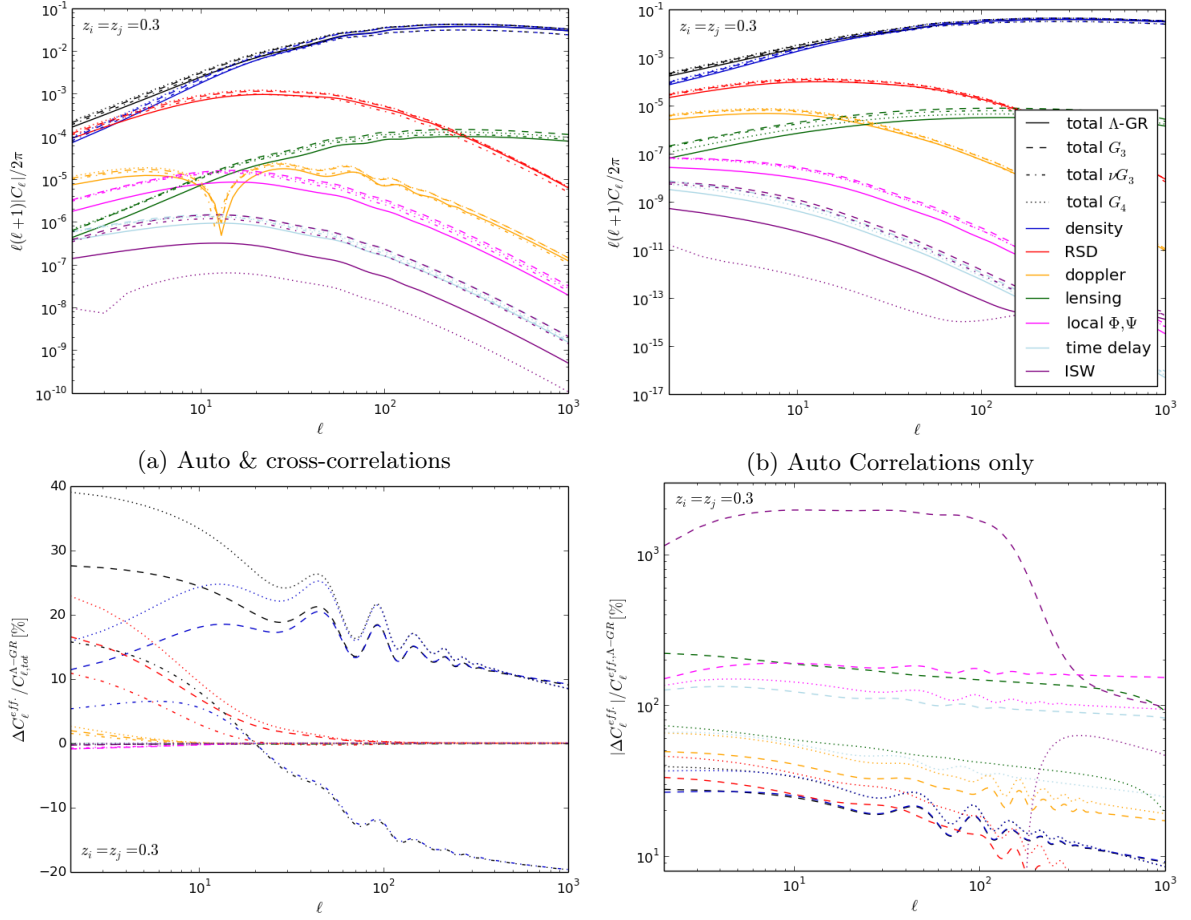


Figure 3: Relativistic effects and total galaxy number count power spectrum for Galileon models and Λ -GR for $z_i = z_j = 0.3$ and tophat window function with bin width 0.05. *Left:* The relativistic effects including their cross-correlation with density is shown. The fractional deviations w.r.t. the total deviation from Λ -GR are plotted in the lower panel. *Right:* pure auto correlations of each effect and their fractional deviation w.r.t. the corresponding effect Λ -GR. Note that we have omitted νG_3 in the fractional deviations for the purpose of distinctiveness. The variations tend to be smaller than in G_3 but of the same order of magnitude. For a better visualization of the lower panels, we use a linear scale on the left and a logarithmic one on the right

correlations on the fixed scale $\ell = 10$ are displayed in [Table 3](#).

The differences in the GNC's between the Galileon models can be understood as follows: adding massive neutrinos to a model introduces the usual suppression of power on small scales due to their free streaming, as it is shown for a cubic Galileon example. This effect partly compensates the enhanced growth. Quartic and quintic Galileons have a higher expansion rate than cubic models leading to increased growth in the matter era. Therefore the dominant local terms, intrinsic density fluctuations, RSD and Doppler terms, are enhanced leading to an increase of the total signal. However, the other sub-dominant effects which depend directly on the Bardeen potentials are less modified than in cubic Galileons as the extra terms reduce the power of the fifth force and therefore the changes to the metric perturbations.

Model	Total	Density	RSD	Doppler	Lensing	Lpot	t-delay	ISW
G_3	24	18 (25)	7 (26)	- (40)	-0.2 (187)	-0.3 (189)	- (123)	- (1964)
G_3	4	-0.4 (-1.1)	3 (9)	- (19)	1.0 (132)	- (84)	- (38)	- (835)
G_3	1.1	-2 (-6)	-2 (-2)	- (-11)	5 (99)	- (23)	- (11)	- (441)
νG_3	8	6 (8)	3 (14)	- (28)	-0.1 (145)	-0.2 (165)	- (105)	- (1460)
νG_3	-5	-4 (-10)	-2 (1.1)	- (8)	0.8 (110)	- (67)	- (39)	- (563)
νG_3	-8	-4 (-15)	-9 (-12)	- (-17)	4 (84)	- (163)	- (16)	- (287)
G_4	33	24 (34)	9 (35)	- (53)	-0.2 (59)	-0.3 (142)	- (56)	- (-99)
G_4	8	1.2 (3)	7 (16)	- (30)	0.5 (64)	- (136)	- (36)	- (-19)
G_4	0.6	-1.2 (-4)	-1.0 (0.2)	- (-7)	3 (56)	- (-22)	- (14)	- (-0.3)
G_5	28	21 (30)	7 (21)	- (37)	-0.2 (91)	-0.2 (109)	- (74)	- (103)
G_5	6	1.0 (3)	5 (11)	- (24)	0.6 (81)	- (79)	- (32)	- (147)
G_5	2	-1.0 (-4)	-0.5 (0.8)	- (-7)	3 (66)	- (5)	- (11)	- (50)

Table 2: Contribution of each effect to the deviation in Equation 4.1 (in percentage). Numbers in parenthesis indicate the relative deviation of each individual effect. First, second and third line represent values for auto-correlations with $z_i = z_j = 0.3, 1$ and 2.5 , respectively. All values show the departure at $\ell = 10$ and consider both auto & cross-correlations with density; Numbers in parenthesis indicate the relative deviation of each individual effect w.r.t. the effect in Λ -GR. “ - ” indicates that the absolute value of the deviations is smaller than 0.1%.

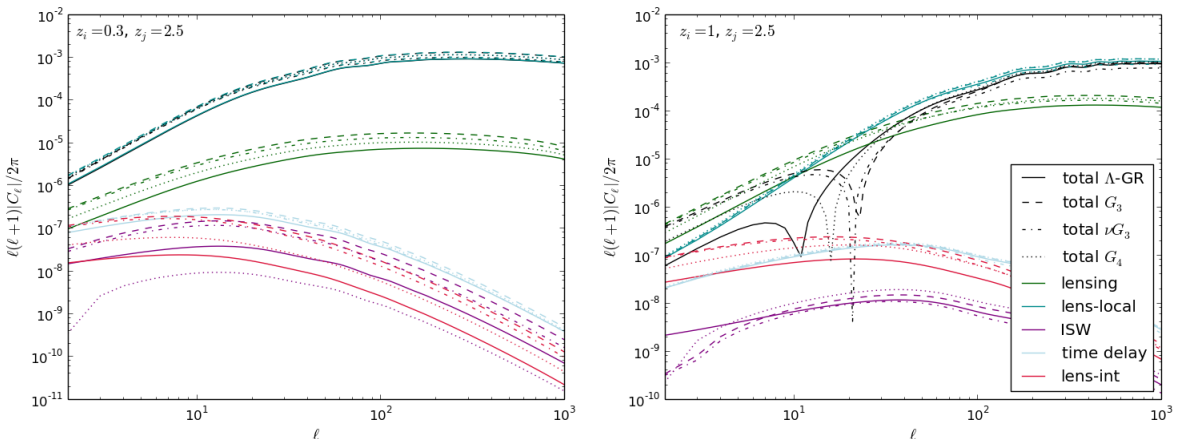


Figure 4: Dominant relativistic effects and total galaxy number count power spectrum for Galileon models and Λ -GR in the correlation of different redshift bins. Time-delay and ISW include their cross-correlation with density. The window function is a tophat with bin width 0.05. The redshift correlations are indicated in the plots. Correlations of the lensing term alone can dominate the signal on the largest angular scales.

4.2 Parameterized Horndeski gravity

We consider now the effects of the different alpha functions from the Bellini-Sawicki parametrisation [37] on the total GNC's and each contribution to it. For this purpose we use models in which the alpha functions are proportional to the energy density of dark energy, i.e.

Model	$z_i - z_j$	Total	Lensing	Lensing-Local	Lensing-Int.	t-delay	ISW
G_3	03-1	61	58 (175)	65 (59)	-0.5 (185)	0.5 (102)	2 (1831)
G_3	0.3-2.5	58	57 (171)	63 (58)	-0.4 (181)	0.2 (97)	0.4 (1619)
νG_3	03-1	45	43 (138)	48 (44)	-0.4 (147)	0.4 (90)	1.4 (1323)
νG_3	0.3-2.5	43	43 (136)	47 (43)	-0.3 (144)	0.2 (88)	0.4 (1173)
G_4	03-1	51	50 (60)	53 (51)	- (62)	0.4 (46)	0.4 (-98)
G_4	0.3-2.5	49	49 (60)	51 (49)	- (61)	0.2 (43)	0.1 (-98)
G_5	03-1	53	52 (90)	55 (53)	-0.2 (94)	0.4 (62)	0.9 (115)
G_5	0.3-2.5	51	51 (89)	53 (51)	-0.2 (92)	0.2 (58)	0.2 (91)

Table 3: Contribution of each effect to the deviation with respect to Λ -GR (in percentage) for different redshift bin correlations. All values show the departure at $\ell = 10$ and consider both auto & cross-correlations with density (apart from the Lensing-Local and Lensing-Integrated cross-correlations); Numbers in parenthesis indicate the relative deviation of each individual effect w.r.t. the effect in Λ -GR. Note that we have omitted $z_i = 1$, $z_j = 2.5$ as the fractional deviations diverge due to the zero crossing of the signal of Λ -GR on this scale.

c_K	c_B	c_M	c_T	w
1	$0.63^{+0.29}_{-0.47}$	0	0	-1
1	$0.92^{+0.40}_{-0.59}$	$1.12^{+0.74}_{-1.46}$	0	-1
1	0	$0.44^{+0.12}_{-0.44}$	0	-1
1	0	$0.61^{+0.19}_{-0.67}$	$0.06^{+0.33}_{-1.04}$	-1
1	0	0	$1/\Omega_{de} < c_T < 0$	-1

Table 4: Constraints on the Horndeski parameterization (3.9), (3.10) using Planck and BOSS-BAO data. Values show the mean and 68% confidence intervals (see also [87]). When errors are not indicated, we fixed the parameter in the analysis. Note that for c_T we have taken the constraints arising purely from stability conditions.

$\alpha_i = c_i \Omega_{de}$, where the α_i 's and c_i 's correspond to kineticity, braiding, running and tensor speed excess, respectively. To make sure we are considering viable theories we run several Markov Chain Monte Carlo analyses using Planck 2015 [91] temperature data and BAO measurements from BOSS [93–95]. Our MCMC analysis showed that the standard cosmological parameters do not vary significantly from the Λ GR values. We have therefore fixed them to the Planck best-fit values [96] when plotting the model predictions. This analysis gives us a baseline of models that produce acceptable CMB spectra and expansion rates but without introducing any information about the matter distribution other than inferred from secondary CMB effects. As we analyse the effects of either one parameter or of a combination of parameters, we run a MCMC for each of the considered combinations. Our results are shown in Table 4.

4.2.1 Kineticity

The kineticity parameterizes the standard kinetic term for the scalar field. It modulates its speed of sound, but does not directly affect the growth of matter or metric perturbations in

any significant way. Hence, we do not expect the GNC's to be sensitive to a variation of c_K . This expectation was corroborated by our results: even for extreme values like $c_K = 10^{\pm 3}$ the fractional deviations w.r.t Λ -GR do not exceed 0.1% on any scale up to $\ell = 1000$ in the $C_\ell(z_i, z_j)$'s for the considered redshifts.

We have also checked if the influence of kinematicity increases when one considers models with an equation of state parameter $w \neq -1$. This allows kinematicity models to have non-zero speed of sound, which is suppressed by $(1 + w)$ in this simple case. Considering a value $w = -0.87$ (2σ away from $w = -1$ [91]) and comparing two models with and without c_K , does not give rise to any significant changes in the GNC's or the relativistic corrections to it. For our further analysis we have fixed the value of c_K to 1 in all considered models.

4.2.2 Tensor Speed Excess

By tuning the tensor speed excess, c_T , one can consider models in which tensor perturbations propagate faster ($c_T > 0$) or slower ($c_T < 0$) than the speed of light. Models with negative values of c_T lead to a slight reduction of power in the matter power spectrum for modes $k \lesssim 10^{-3}h/Mpc$. Modifications to the metric perturbations also only start becoming relevant on scales close to the horizon. On these scales the tensor speed excess introduces anisotropic stress and a negative value of c_T causes an increase of Φ while Ψ is decreased w.r.t. Λ -GR in the dark energy dominated era. The effect on Ψ is larger than the effect on Φ such that the lensing potential, $\Phi + \Psi$, is reduced.

The decrease of matter perturbations and of the lensing potential are reflected in the GNC's. The dominating local effects, the lensing magnification and the time-delay are slightly decreased. Only the ISW is decrease for small redshifts while it is enhanced for high redshifts. However, the modifications to the total signal are very small (below 1%) on all scales up to $\ell = 1000$ for all considered redshift bin correlations $z_i = z_j$ and $z_i \neq z_j$, even for large values of the tensor speed excess ($c_T = -0.9$).

4.2.3 Running effective Planck Mass

In this section we first consider the influence of a running of the effective Planck mass (“running”) on the GNC's and then models with both, running and tensor speed excess.

A positive running rate causes an effective increase of the gravitational constants at late time, implying more clustering. Therefore the power of the matter power spectrum is enhanced on ultra-large scales ($k \lesssim 10^{-3}h/Mpc$). Considering the metric perturbations it causes Φ to decrease and Ψ to increase on sub horizon scales, where the effect on Φ is stronger such that the lensing potential is decreased. The evolution of both potentials is faster than in Λ -GR such that the curves are tilted stronger.

In the GNC's the increase of the matter power translates to an enhancement of the density fluctuations, RSD and Doppler effects. On the other hand, the decreased lensing potential leads to and reduction of the lensing magnification and the Shapiro time-delay contributions w.r.t. Λ -GR. Through the larger tilt of the Bardeen potentials the ISW, which depends on their derivatives, gets enhanced. We show the total GNC's and all relativistic contributions to it for $z = 0.3$ in Figure 5 for Λ -GR and a model with $c_M = 0.68$, which corresponds to the mean of our MCMC plus 2σ . In the *upper left panel* we show each effect and its cross-correlation with density. The *lower left* shows the fractional deviation of each effect w.r.t. the total GNCs of Λ -GR. The pure effects and their fractional deviation w.r.t. to the corresponding effect in Λ -GR are shown in the *right panel*. It shows that the ISW effect is the most sensitive effect to a variation of c_M . But even though the integrated effects

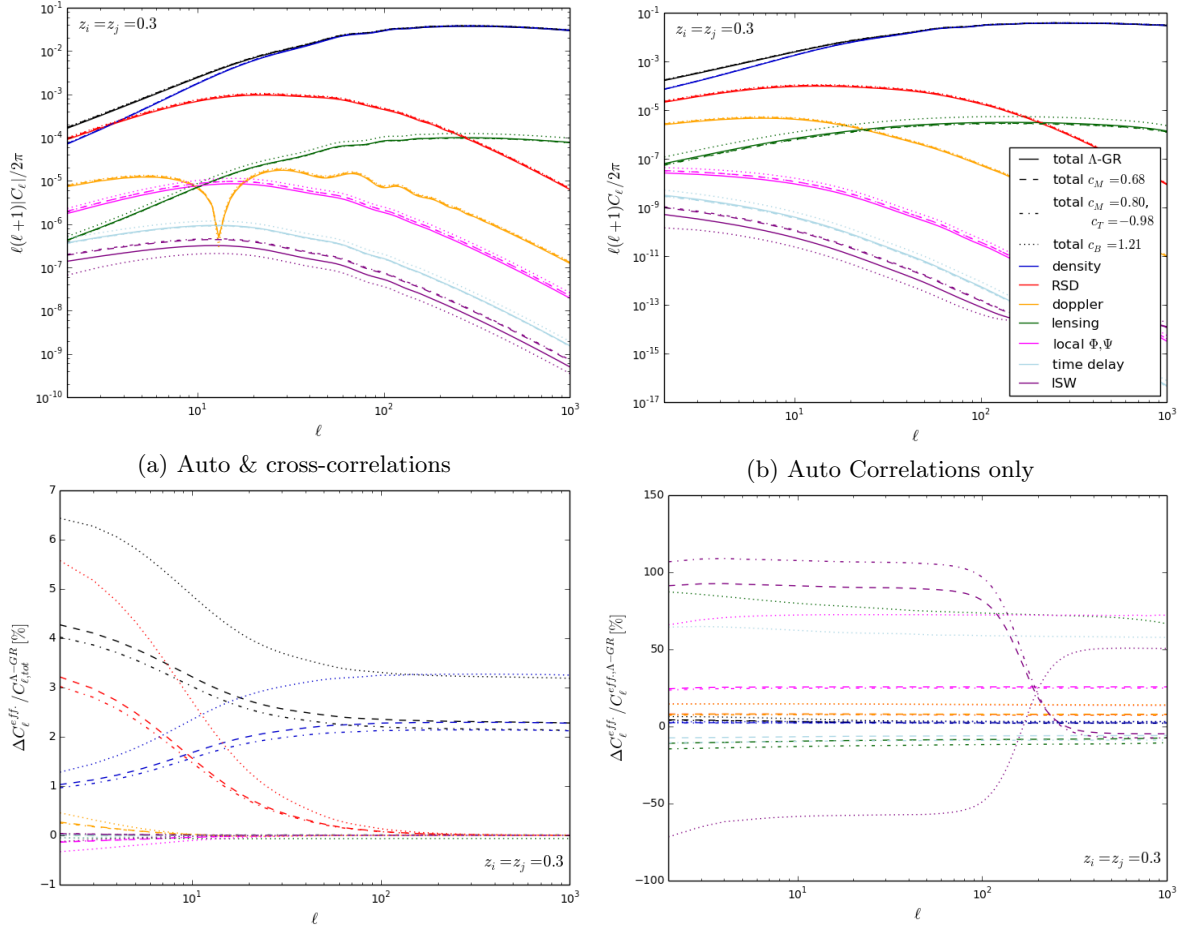


Figure 5: Relativistic effects and total galaxy number count power spectrum for different parameterized models and Λ -GR for $z_i = z_j = 0.3$. *Left:* The relativistic effects including their cross-correlation with density is shown. The fractional deviations w.r.t. the total deviation from Λ -GR are plotted in the lower panel. *Right:* pure auto correlations of each effect and their fractional deviation w.r.t. the corresponding effect Λ -GR. In each case we used a tophat window function with bin width $\Delta = 0.05$.

can be modified significantly, the effect on the total GNC's $C_\ell(z_i, z_i)$ is only small (lower left panel).

In different redshift bin correlations the enhanced impact of the lensing magnification causes a stronger modification of the total signal, see [Figure 6](#). It is about 20 % on all scales up to $\ell = 1000$ for $c_M = 0.68$ in the configuration $z_i = 0.3, z_j = 2.5$ (*left panel* of [Figure 6](#)). The *right panel* shows the contributions to GNC's for for $z_i = 1, z_j = 2.5$. Here, the slight enhancement of the local terms and the decrease of the lensing magnification shifts the scale on which both effects cancel each other out. The sign change of the total signal is therefore shifted towards smaller scales (larger ℓ) for larger values of c_M .

Models with a negative run rate of the effective Planck mass have instabilities associated to a negative speed of sound ([Equation 3.7](#)), leading to diverging values of the scalar field on the scales we are considering. Therefore it is necessary to introduce - at least - one other non zero component in addition to c_K and c_M . In this light we also analyse how a combination of

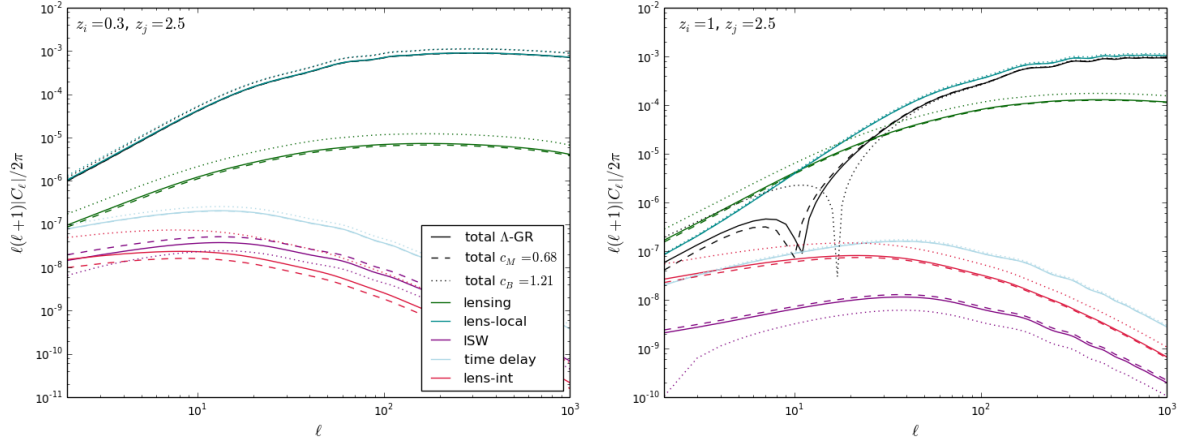


Figure 6: Dominant relativistic effects and total galaxy number count power spectrum for parameterized Horndeski models and Λ -GR for different redshift bin correlations. Time-delay and ISW include their cross-correlation with density. The window function is a tophat with bin width 0.05. The redshift bins are indicated in the plots. Note that in the case of $z_i = 1, z_j = 2.5$ the signal can even be dominated by the lensing correlations alone on the largest scales.

the running effective Planck mass and the tensor speed excess affect the perturbations and the GNC's.

In the configuration with $c_M \neq 0$ an introduction of a negative tensor speed excess has the same influence on the perturbations for sub horizon modes as before for $c_M = 0$. The reduction of the matter power and the lensing potential lead to a decrease of the leading local contributions and the lensing potential. This can be seen very well in the lower panels of [Figure 5](#) when comparing the two models with c_M : as discussed, an increase of c_M leads to an increase of the density, RSD and Doppler contributions, but with tensor speed excess these effects are decreased even w.r.t. a model with smaller c_M but $c_T = 0$.⁹

For the ISW the behaviour is more complex. Modifications of c_T have a larger impact for higher redshifts which is opposite to the effects of c_M , see the first two models in [Table 5](#). In combination the presence of the running boosts the impact of the tensor speed excess to become larger for high redshifts. Instead of being decreased for a model with only running, the ISW in combination with its cross-correlation with density gets increased for high redshifts by the tensor speed excess, see third model in [Table 5](#). This opens a window to potentially distinguish between models with and without c_T .

Besides that, it is interesting to notice that considering small modes for a fixed, positive c_M , Ψ gets decreased and Φ increased independently of the sign of c_T . However, on modes near the horizon this behaviour is interchanged only negative values of c_T (Ψ is increased while Φ is decreased). Furthermore, fixing c_M , the modifications on the GNC's are stronger for models with tensor modes propagating faster than the speed of light compared to models in which they propagate subluminal.

⁹The model $c_M = 0.9$ and $c_T = -0.98$ corresponds to the mean $c_M + 1\sigma$ and mean $c_T - 1\sigma$ of our MCMCs. For each parameter we have taken the bound which is further away from standard gravity, i.e. $c_i = 0$, and 1σ values to avoid tensor instabilities due to $1 + \alpha_T < 0$.

Model	$z_i = z_j$	ISW	ISW + Dens-ISW
$c_T = -0.98$	0.3	-0.05	-0.08
$c_T = -0.98$	1	-0.2	-0.1
$c_T = -0.98$	2.5	0.3	4
$c_M = 0.8$	0.3	112	45
$c_M = 0.8$	1	76	18
$c_M = 0.8$	2.5	58	-3
$c_M = 0.80, c_T = -0.98$	0.3	108	44
$c_M = 0.80, c_T = -0.98$	1	80	24
$c_M = 0.80, c_T = -0.98$	2.5	68	14

Table 5: Fractional deviations in % of ISW effect and its cross-correlation with density in auto-bin correlations relative to the corresponding effects in Λ -GR for $\ell = 10$.

4.2.4 Braiding

In contrast to models with a running of the effective Planck mass or tensor speed excess, braiding models do not incorporate anisotropic stress. Both Bardeen potentials get enhanced in the same manner w.r.t. Λ -GR and can stay constant even after matter domination for values $c_B \sim 0.8$ ($c_K = 1$). While the metric perturbations are enhanced for all modes the matter perturbations are scale dependent. The matter power spectrum is slightly enhanced on small scales ($k \gtrsim 2 \cdot 10^{-3} h/Mpc$) for positive values of c_B while it is decreased on larger scales.

The enhanced growth of matter perturbations on sub horizon scales for models with positive braiding leads to an increase of the dominant local terms. Hence the total signal gets enhanced of about 6% for the mean $c_B + 2\sigma$ from our MCMCs ($c_B = 1.21$, $c_K = 1$). With the increase of the metric perturbations the lensing potential, and thereby the lensing magnification and the Shapiro time-delay, are enhanced as well. For higher redshifts the contribution of the lensing magnification to the total signal gets more important and the deviations of the total GNC's can be dominated by the enhancement of lensing. For example in the considered braiding model for $z = 2.5$ the lensing contribution is increased by $\sim 50\%$ which leads to an enhancement of the total signal of order 5%. The ISW effect gradually decreases with an increase of c_B and can almost vanish for the case were the Bardeen potentials stay approximately constant even after matter domination ($c_B \sim 0.8$). Increasing c_B further leads to a change of sign in the ISW as the potential will increase in the dark energy dominated era instead of decrease as in Λ -GR. Therefore the ISW effect is the one which is most sensitive to a change of c_B . All relativistic effects and their deviations from Λ -GR for this model are shown in [Figure 5](#) for $z = 0.3$.

A variation of braiding also leaves signatures in different redshift bin correlations. Due to the enhancement of the lensing magnification the cross-correlations between lensing and local as well as lensing and integrated effects are also increased. As these are the dominant contributions this can lead to an increase of the total signal of $\sim 20\%$ on all scales for $c_B = 1.21$. Another effect is that in configurations with a sign change of the total GNC's the signal can be several orders of magnitude larger or smaller w.r.t. Λ -GR. This is the case as the negative cross-correlation between lensing and the local terms gets less enhanced than the pure lensing magnification contribution. Therefore the scale where this two effects

cancel out is shifted towards smaller scales when increasing c_B (and therefore the lensing magnification). For models with negative braiding the lensing potential is decreased and the shift is towards larger scales. We stress that for the detection of this effect, observational factors, like the magnification bias term $2 - 5s(z)$ entering in eq. (2.9), also influence the sign of the lensing-local cross-correlation and have to be taken into account (we have set $s = 0$ here).

In combinations of braiding with tensor speed excess or a running effective Planck mass only the terms which do not directly depend on the Bardeen potentials, namely density fluctuation, RSD and Doppler, show the expected behaviour from the previous sections when varying one parameter while the others are kept constant. For the other contributions the dependencies are not as trivial anymore. The modifications on the Bardeen potentials strongly depend on the specific values of c_B and c_T or c_M and can not any longer be related to obvious effects, e.g. a change of sign of one parameter. Furthermore the introduction of anisotropic stress with c_T or c_M leads to additional variations. Therefore the modifications to the relativistic effects depending on the Bardeen potentials in the combined cases are more subtle and have to be analysed for the specific cases.

5 GNC-CMB temperature correlation in Horndeski gravity

We have found that the relativistic effects involving integrals along the line of sight deviate significantly from the Λ -GR across the models under study. Fortunately, it is possible to isolate one of such effects by considering cross-correlation of LSS with the CMB temperature anisotropies. This measurement is dominated by the ISW effect in the CMB, which has the same dependence on the potentials as the ISW in GNC. This provides a perfect set-up to test the viability of modified gravity models: in fact, our analysis in section 4 has shown that the ISW effect is the effect which is most sensitive to the underlying theory of gravity. We start by giving a short overview of the theoretical foundations. Then we explore which regions of the parameter space of the Bellini-Sawicki parameterization predict viable values for the CMB-LSS correlation. The measurements we use have been obtained by Ferraro, Sherwin and Spergel [24] using data from the WISE survey [30].

The time variation of the Bardeen potentials causes a fractional variation in the CMB temperature [97] which is given by

$$\left(\frac{\Delta T}{T}\right)_{ISW} = \int d\tau (\Phi' + \Psi'). \quad (5.1)$$

The potentials are constant in the matter dominated era and therefore there are no contributions to the ISW effect from this time. It can be only caused by post-recombination radiation, where the matter over-density was very small, or in the dark energy dominated era ($z \lesssim 1$). Therefore the major impact on the ISW effect comes from ultra-large scales. Even though it is subdominant in the CMB temperature-temperature anisotropy spectrum, the ISW effect can be isolated considering the cross-correlation between the CMB temperature and galaxy number counts. The angular power spectrum of this cross-correlation can be computed by assuming that the ISW effect is the only contribution at low redshifts, such that:

$$C_\ell^{Tg} \approx C_\ell^{\dot{\Phi}g} = 4\pi \int \frac{dk}{k} \Delta_m^2(k, z=0) K_\ell^{\dot{\Phi}}(k) K_\ell^g(k), \quad (5.2)$$

where $\Delta_m^2(k, z=0) = k^3 P(k, z=0)/2\pi^2$ is the dimensionless (linear) matter power spectrum and the weight functions

$$K_\ell^g(k) = \int dz b(z) \frac{dN}{dz} D(z) j_\ell(x) \quad (5.3)$$

$$K_\ell^\Phi(k) = \frac{3\Omega_m H_0^2}{k^2} \int dz \frac{d}{dz} ((1+z)D(z)) j_\ell(x). \quad (5.4)$$

with the linear growth factor $D(z)$ (normalized to 1 at $z=0$) and the spherical Bessel functions j_ℓ with the comoving distance $x \equiv k(\tau_0 - \tau)$ as argument. Furthermore a linear bias model for tracers is assumed and the redshift distribution dN/dz is normalized such that $\int dz' \frac{dN}{dz'} = 1$.

The viability of a gravity model can be tested through CMB-LSS correlations by constraining the *CMB-LSS relative amplitude*

$$\mathcal{A} = \frac{\sum_\ell C_\ell^{Tg}(MG)}{\sum_\ell C_\ell^{Tg}(\text{ref})} \quad (5.5)$$

defined with respect to the Planck best fit model [91]. Analysing WISE data [30] Ferraro et al. [24] found it to be $\mathcal{A} = 1.24 \pm 0.47$. This measurement can be used to further rule out covariant Galileon models, as they would predict a negative correlation [29]. To see if the parameterized Horndeski models we used can also be constrained or ruled out by this observation we added the CMB-LSS correlations to `hi_class`. In the following we will compute the amplitude \mathcal{A} using a tophat window function centered around $z=0.3$ (the central redshift of WISE galaxies) with bin width $\Delta = 0.05$. As we are interested in a rough estimate, given the relatively small width of the redshift bin we neglect the evolution of galaxy bias and of the galaxy selection function, and assume that they factor out in the ratio. Also, since Equation 5.5 was constrained in [24] by considering all the WISE galaxies up to $z=1$, caution should be taken when comparing our results to their measurement.

Figure 7 shows the CMB-LSS cross-correlation for covariant Galileons and parameterized models for redshift $z=0.3$ and their corresponding values for the amplitude \mathcal{A} . This plots are in perfect agreement with our previous results. The CMB-LSS cross-correlation is enhanced for models with a positive run rate of the effective Planck mass, i.e. $c_M > 0$, as the ISW is increased with increasing c_M . In models with positive braiding the signal is reduced w.r.t. Λ -GR as the ISW is decreased for increasing c_B . We have omitted models with only kineticity or tensor speed excess from the plots as they barely influence the signal, as expected from the ISW analysis in the GNC's.

The *left panel* of Figure 8 shows the value of the CMB-LSS amplitude (Equation 5.5) in the $c_B - c_M$ plane of parameterized Horndeski models. The effect of the braiding is to lower the amplitude, eventually leading to negative values of \mathcal{A} for $c_B \gtrsim 0.8$. The running of the effective Planck mass has the opposite effect, increasing the signal beyond the Λ -GR prediction and doubling its value for $c_M \gtrsim 1.5$. The two parameters have the opposite effect, leading to net cancellation roughly coinciding with $c_M \approx 2c_B$. This degeneracy in the ISW-LSS prediction leads to a relatively large region of the parameter space compatible with the measured value of \mathcal{A} . Note that the degeneracy would allow one to distinguish first generation of scalar-tensor theories (i.e. Jordan-Brans-Dicke, $f(R)$, quintessence, K-essence in which $\alpha_B = -\alpha_M$ from Horndeski models with more general α_B, α_M).

The influence of a tensor speed excess gets substantial when combined with braiding or running, even though it has no significant impact on the CMB-LSS correlation if α_B and

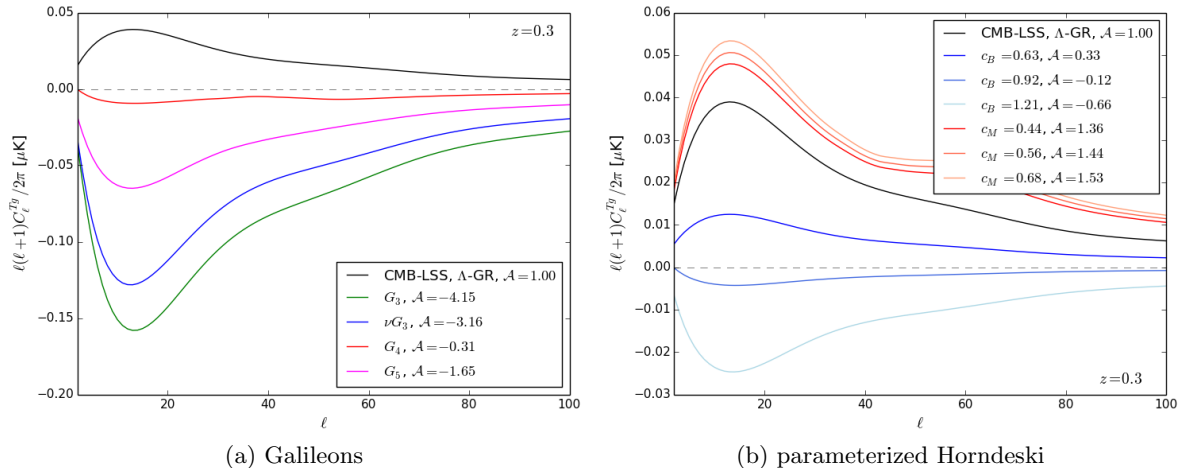


Figure 7: Cross-correlation between large scale structure and CMB temperature anisotropies for Galileon models (*left*) and parameterized Horndeski models (*right*) in comparison to Λ -GR for redshift $z = 0.3$ with tophat window function and bin width 0.05; note that $c_K = 1$ in all parameterized models.

α_M are both zero. In combination with the considered braiding model, $c_B = 1.21$, a negative tensor speed excess, e.g. $c_T = -0.98$, causes the CMB-LSS correlation to be reduced at low redshifts ($z \sim 0.3$) compared to a model with $c_B = 1.21$ but $c_T = 0$. This reduction at $z = 0.3$ is of order 5% on the scale $\ell = 50$. For high redshifts ($z \gtrsim 1$) the tensor speed excess causes an enhancement of the signal and the effect is considerably stronger. In the given example this increase is about 95% at redshift $z = 2.5$ and scale $\ell = 50$.

In the case of a combination of c_T and c_M the behaviour is similar. A negative value of c_T just slightly influences the CMB-LSS correlation for low redshifts but has a larger impact on higher redshifts, as discussed in 4.2.3. E.g. the signal is increased w.r.t. Λ -GR for $c_M = 0.8$ without tensor speed excess but decreased when $c_T = -0.98$ at redshift $z = 2.5$. In contrast to that c_T slightly enhances the signal for low redshifts, see the *right panel* of Figure 8 where we plot the amplitude of the CMB-LSS correlation in the $c_M - c_T$ plane for $z = 0.3$. At this redshift the effect is only small ($\sim 0.5\%$) while it is more significant ($\sim 11\%$) for $z = 2.5$ at scale $\ell = 50$, when comparing the two models with and without tensor speed excess. This feature can be used to isolate the impact of the propagation speed of gravitational waves by comparing the CMB-LSS cross-correlation at different redshifts, as the impact of α_T is strongly increased for high redshifts.

6 Conclusions

We have systematically studied the impact of consistent, alternative theories of gravity on LSS observations involving ultra-large scales. Our theoretical landscape is given by models within the Horndeski Lagrangian, a very general theory that encompasses many viable models for dark energy and modified gravity. Among these models, we have focused on covariant Galileons and the minimal parameterization of the dynamics proposed by Bellini and Sawicki, using the `hi_class` code¹⁰ [38] to obtain predictions for the observable quantities in the linear regime. Our work is the first to explore this regime of structure formation using fully

¹⁰www.hiclass-code.net

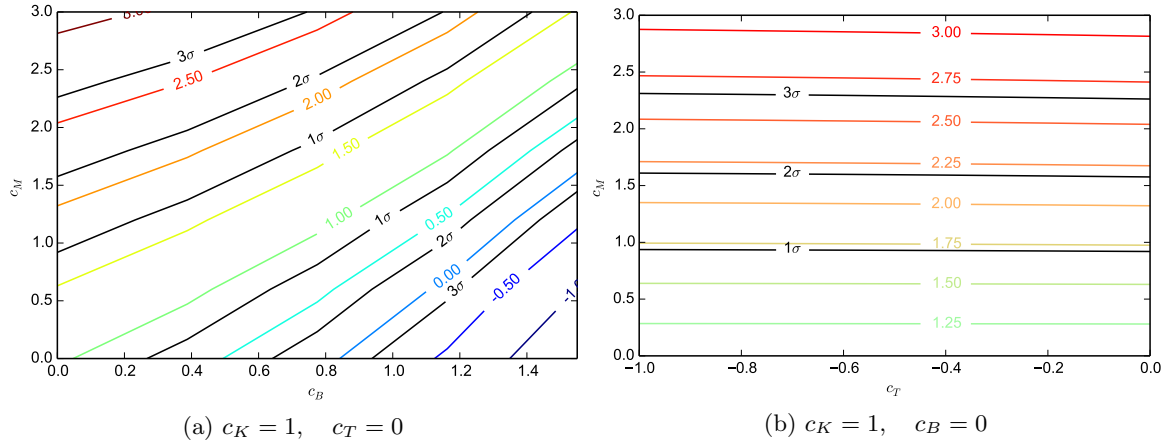


Figure 8: Cross-correlation between large scale structure and CMB temperature anisotropies for the Bellini-Sawicki parameterization (cf. section 3.2) around the Planck best fit values for Λ -GR. Coloured lines show the values of the relative CMB-LSS relative amplitude (5.5); black lines show the 1,2 and 3 σ deviations with respect to the measured value $\mathcal{A} = 1.24 \pm 0.47$ [24]. Note that large values of the braiding can neutralize the ISW-LSS cross-correlation or even turn it into an anti-correlation.

consistent models in this very general class and is complementary to previous studies that use either parameterizations of the solutions (inspired by quasi-static results), cf. [39, 40], or focus on very specific models [26–28]. We also extend previous analyses of relativistic effects in modified gravity by considering correlations of the galaxy distribution at different redshifts.

As a first observable we have considered power spectra of galaxy number counts. In a relativistic framework, GNC’s depends not only on the intrinsic clustering and RSD terms, but also on other effects non-negligible on the largest scales $k \sim \mathcal{H}$. At least part of those will be detectable by future experiments [14, 15]. These contributions to GNC’s depend directly not only on the growth of matter, but also on the gravitational potentials, making them direct probes of modifications of gravity. Moreover, the possibility of choosing different redshift and angular configurations (e.g. correlating galaxies in the same or different redshift bins) allows one to separately measure some combinations of the relativistic effects.

Correlations of galaxies at the same redshift are dominated by the density contribution, followed by Kaiser-RSD, doppler terms/lensing magnification (depending on the angular scale), local potentials, time-delay and ISW effects [9]. Modified gravity does not significantly alter this hierarchy, in which each contribution is roughly a factor 5-10 smaller than the preceding one, with the exception of swapping the ISW and time delay in some models. The impact of modified gravity is largest on the least dominant contributions, and the discrepancies with respect to Λ -GR are usually dominated by the density and Kaiser RSD.

Considering galaxy correlations at different redshift increases the sensitivity to the theory of gravity. In this configuration the contribution from lensing magnification is particularly important: it can even dominate the signal and therefore the deviations on the largest scales, specially if broad redshift bins are considered [13, 16]. The total deviations can become of order $\sim 40\%$ for covariant Galileons in which the expansion history and the gravitational force are modified. For parameterized models with standard expansion histories they are typically small as the modifications to the leading terms, density and RSD, are minor. But if

large enough redshift bins are considered lensing effects can become important and, with very precise measurements on ultra-large scales (e.g. using multiple tracers), even modifications due to the other sub-dominant relativistic effects might be detectable. It is important to notice that the aforementioned lensing effect is only due to magnification: it does not require measuring galaxy shapes and it is therefore subject to completely different systematics than the usual weak lensing measurements.

The contributions most sensitive to modified gravity are those that involve integrals along the line of sight, namely lensing magnification, Shapiro time delay and the integrated Sachs-Wolfe effect. The sum of these contributions can be isolated by correlating the galaxy distribution in different, non-overlapping redshift bins. In alternative theories of gravity, the balance between the contributions is modified with respect to Λ -GR due to the strong enhancement of the integrated terms: in Horndeski models the contribution from the cross-correlation of lensing with the other integrated terms (i.e. lensing-ISW and lensing-time-delay) can overcome the contribution from the Shapiro time-delay to be the third largest. The two leading terms are the lensing magnification itself and the cross-correlation of lensing with local terms. In Galileons models the lensing-integrated terms correlation can even overcome the latter contribution to be the second largest effect and by itself become larger than the total signal in standard gravity. Although the signal is small, effects such as the lensing magnification will be relevant for future surveys such as Euclid [13] and could provide a novel test of gravity.

The integrated effects have the additional advantage of being sensitive to a broad range of radial scales. This dependence can potentially allow LSS observations at high redshift (for which $\Omega_{de}(z) \ll 1$) to obtain information about dark energy, in a manner analogous to proposals for wide angle weak lensing in 21cm surveys [98, 99]. In addition, higher redshift observations contain more modes comparable to the Hubble horizon in that epoch and are likely to make these effects more important. This “memory” of DE in integrated effects and the increased number of horizons might enable new means to test gravity with high-redshift surveys.

We investigated in detail the effects of non-standard gravity on each contribution to the GNC in the context of the Bellini-Sawicki parameterization [37]. While varying the kineticity parameter and the tensor speed excess alone does not bring substantial changes to the GNC’s, changes in the running of the effective Planck mass and of the braiding parameter leads to significant deviations. A positive run rate causes an effective increase of matter clustering at late times, but a decrease of the lensing potential w.r.t. Λ -GR. In pure braiding models both metric potential are enhanced (but without leading to an anisotropic stress), which is particular interesting for different redshift correlations dominated by integrated terms. Further non-trivial dependencies appear in the GNC’s when the Horndeski parameters are varied jointly.

We have found that the ISW effect is the most sensitive to the theory of gravity, deviating from Λ -GR by as much as 90% for parameterizations and up to 2000% for covariant Galileons. While this effect is negligible in GNC’s, it can be isolated by cross-correlating galaxy catalogues with CMB temperature maps. This correlation has been measured to be positive and in good agreement with the Λ -GR prediction. However, in the majority of the models we have considered the ISW effect can turn to an anti-correlation between CMB temperature and LSS, as it is the case of all best-fit Galileons and models with significant braiding. This dramatic difference exemplifies the power of combining CMB and LSS to probe the nature of gravity.

We can gain further insights into the connection between the ISW effect and the fundamental properties of gravity by means of parameterized models. Our results show that an increase in the effective Planck mass with time, α_M , tends to increase the magnitude of the correlation, while a kinetic mixing between the metric perturbations and the scalar field, α_B , tends to decrease its value and can potentially make it negative. This naturally leads to a degeneracy in the direction $\alpha_B \approx 2\alpha_M$ on which C_ℓ^{Tg} remains close to the standard value. The anomalous propagation of gravitational waves, α_T , can be isolated from other modified gravity effects by comparing the CMB-LSS correlation for different redshifts. α_T in combination with α_M causes a slight decrease of the signal on low redshifts and an increase at higher redshifts compared to models with $\alpha_T = 0$, while we observe the inverse trend in models with braiding.

Future galaxy surveys will hunt for relativistic effects in cosmological observables as yet another confirmation of Einstein theory. These observations offer an excellent opportunity to test gravity in a regime that is naturally at the same dynamical scale as cosmic acceleration. We have studied the impact of consistent modifications of gravity in this regime, paving the way to more specific studies of how these effects can be observationally detected. A very promising technique in this direction is the use of multiple tracers of the LSS distribution, either to reduce cosmic variance or to measure the anisotropic correlation function, directly related to sub-dominant contributions. Cross-correlation between LSS and CMB temperature allows one to isolate the ISW effect and provides a clean, direct test of the properties of gravity. Other cross-correlations between different field are also possible and might provide complementary signatures [100].

Another avenue for further development can be pursued by considering more general theoretical frameworks. Beyond Horndeski theories of the G^3 type [62] have characteristic signatures that vanish in the quasi-static regime [101]. This might be more critical to test degeneration models that address the cosmological constant problem, often leading to signatures only on curvature regime comparable to the residual Λ [102]. These observational prospects and theoretical developments anticipate a new era in which large-volume galaxy surveys will bring in new insights into fundamental physics and the nature of gravity.

Acknowledgements: We are very grateful to Luca Amendola for initial discussions and many useful suggestions along the way, David Alonso and Ruth Durrer for comments on the draft, Daniele Bertacca, Enea Di Dio, and Alvise Raccanelli for discussions of relativistic effects, as well as Simone Ferraro and Laura Taddei for discussions on the ISW effect. JR and MZ are partially supported is supported by DFG through the grant TRR33 “The Dark Universe”. JR acknowledges support from Stockholm University and the Oskar Klein Center.

A Transfer functions

We compute the linear transfer functions of relativistic number counts with `hi_class`¹¹ [38] a modified version of the CLASS code¹² [103], based on the implementation introduced in CLASSGAL¹³ [104]. For more details see, e.g., [9, 10, 104].

¹¹<http://hiclass-code.net/>

¹²<http://class-code.net/>

¹³<http://cosmology.unige.ch/content/classgal>

The transfer functions read:

$$\begin{aligned}
\Delta_\ell^{\text{Den}_i} &= \int_0^{\tau_0} d\tau W_i b(z) S_\delta j_\ell \\
\Delta_\ell^{\text{Len}_i} &= \ell(\ell+1) \int_0^{\tau_0} d\tau W_i^{\text{L}} S_{\Phi+\Psi} j_\ell \\
\Delta_\ell^{\text{V1}_i} &= \int_0^{\tau_0} d\tau W_i \left[1 + \frac{H'}{aH^2} + \frac{2-5s}{(\tau_0-\tau)aH} + 5s - f_{\text{evo}} \right] \frac{S_\Theta}{k} \frac{dj_\ell}{dx} \\
\Delta_\ell^{\text{V2}_i} &= \int_0^{\tau_0} d\tau W_i (f_{\text{evo}} - 3) aH \frac{S_\Theta}{k^2} j_\ell \\
\Delta_\ell^{\text{V3}_i} &= \int_0^{\tau_0} d\tau W_i \left(\frac{1}{aH} \right) S_\Theta \frac{d^2 j_\ell}{dx^2} \\
\Delta_\ell^{\text{G1}_i} &= \int_0^{\tau_0} d\tau W_i \left[c_{\text{lpot}} + (c_{\text{lpot}} - c_{\text{isw}}) \left(1 + \frac{H'}{aH^2} + \frac{2-5s}{(\tau_0-\tau)aH} + 5s - f_{\text{evo}} \right) \right] S_\Psi j_\ell \\
\Delta_\ell^{\text{G2}_i} &= \int_0^{\tau_0} d\tau W_i \left[(c_{\text{lpot}} - c_{\text{isw}})(-2+5s) - c_{\text{isw}} \left(3 + \frac{H'}{aH^2} + \frac{2-5s}{(\tau_0-\tau)aH} - f_{\text{evo}} \right) \right] S_\Phi j_\ell \\
\Delta_\ell^{\text{G3}_i} &= c_{\text{lpot}} \int_0^{\tau_0} d\tau W_i \left(\frac{1}{aH} \right) S_{\Phi'} j_\ell \\
\Delta_\ell^{\text{G4}_i} &= c_{\text{std}} \int_0^{\tau_0} d\tau W_i^{\text{G4}} S_{\Phi+\Psi} j_\ell \\
\Delta_\ell^{\text{G5}_i} &= c_{\text{isw}} \int_0^{\tau_0} d\tau W_i^{\text{G5}} S_{(\Phi+\Psi)} k \frac{dj_\ell}{dx}, \tag{A.1}
\end{aligned}$$

where for the integrated terms we defined

$$\begin{aligned}
W_i^{\text{L}}(\tau) &= \int_0^\tau d\tilde{\tau} W_i(\tilde{\tau}) \left(\frac{2-5s}{2} \right) \frac{\tau - \tilde{\tau}}{(\tau_0 - \tau)(\tau_0 - \tilde{\tau})} \\
W_i^{\text{G4}}(\tau) &= \int_0^\tau d\tilde{\tau} W_i(\tilde{\tau}) k \frac{2-5s}{\tau_0 - \tilde{\tau}} \\
W_i^{\text{G5}}(\tau) &= \int_0^\tau d\tilde{\tau} W_i(\tilde{\tau}) \left[1 + \frac{H'}{aH^2} + \frac{2-5s}{(\tau_0 - \tilde{\tau})aH} + 5s - f_{\text{evo}} \right]_{\tilde{\tau}}. \tag{A.2}
\end{aligned}$$

Here the source functions $S_X(k, \tau)$ are linear combinations of transfer functions $A(\tau, k) \equiv A(\tau, \mathbf{k})/\mathcal{R}(\tau_{\text{ini}}, \mathbf{k})$, where $A(\tau, \mathbf{k})$ is any perturbation with adiabatic initial conditions, and $\mathcal{R}(\tau_{\text{ini}}, \mathbf{k})$ is the curvature perturbation at some initial time τ_{ini} such that the corresponding mode is super horizon $k\tau_{\text{ini}} \ll 1$. We integrate over a window function $W(z_i)$ centered at redshift z_i that encodes information about the redshift resolution (typically a tophat for spectroscopic resolution, or a Gaussian with variance given by photometric resolution) and about the distribution of galaxies per redshift and per solid angle $dN/dz/d\Omega$. We omitted the arguments k for the transfer functions Δ , (τ, k) for the source functions S_X , $x \equiv k(\tau_0 - \tau)$ for the Bessel functions j_ℓ (τ_0 being the conformal time today), and τ for selection and background functions. We also introduced the velocity source function $S_\Theta(\tau, k)$ given by $\Theta(k) \equiv kV(k)$, where $V(k)$ is the velocity perturbation in the Newtonian gauge. Primes indicate derivatives with respect to conformal time. In the following paragraph we describe the newly introduced coefficients c_{isw} , c_{std} and c_{lpot} added to identify the ISW, Shapiro time-delay and other local terms depending on the Bardeen potentials, respectively. These coefficients allow us a more physical description of the relativistic terms $\Delta_\ell^{\text{G}^i}$, while still

splitting the contributions in the code according to their source function and number of derivatives of spherical Bessel functions.

The different contributions shown above correspond to the density in comoving gauge δ_{co} (“Den”), lensing convergence κ (“Len”), Doppler (“V1”-“V2”), redshift-space distortions in the Kaiser approximation (“V3”) and terms depending on gravitational potential (“G1”-“G5”), respectively. The separation of different contributions is consistent with the CLASS code. In particular, it differs from the previous CLASSGAL implementation as, for numerical convenience, the time derivative Ψ' (requiring numerical derivatives of perturbation equations) has been integrated by parts. The corresponding expressions for the relativistic transfer functions (other than lensing convergence) presented in CLASSGAL [104] are

$$\begin{aligned}
\Delta_{\ell}^{\widetilde{G1}_i} &= c_{\text{lpot}} \int_0^{\tau_0} d\tau W_i \left(2 + \frac{H'}{aH^2} + \frac{2-5s}{(\tau_0-\tilde{\tau})aH} + 5s - f_{\text{evo}} \right) S_{\Psi} j_{\ell} \\
\Delta_{\ell}^{\widetilde{G2}_i} &= c_{\text{lpot}} \int_0^{\tau_0} d\tau W_i (-2 + 5s) S_{\Phi} j_{\ell} \\
\Delta_{\ell}^{\text{G3}_i} &= c_{\text{lpot}} \int_0^{\tau_0} d\tau W_i \left(\frac{1}{aH} \right) S_{\Phi'} j_{\ell} \\
\Delta_{\ell}^{\text{G4}_i} &= c_{\text{std}} \int_0^{\tau_0} d\tau W_i^{\text{G4}} S_{\Phi+\Psi} j_{\ell} \\
\Delta_{\ell}^{\widetilde{G5}_i} &= c_{\text{isw}} \int_0^{\tau_0} d\tau W_i^{\text{G5}} S_{(\Phi'+\Psi')} j_{\ell} ,
\end{aligned} \tag{A.3}$$

where a tilde $\widetilde{G}i$ indicates expressions proper of CLASSGAL. Equations (A.1), implemented in CLASS, are recovered once we integrate by parts $\Delta_{\ell}^{\widetilde{G5}_i}$ (neglecting boundary terms since they vanish as $\tau \rightarrow 0$ and are unobservable for $\tau = \tau_0$) and redefining consistently $\Delta_{\ell}^{\widetilde{G1}_i}$ and $\Delta_{\ell}^{\widetilde{G2}_i}$ such that the sum of these three terms is unchanged. It is worth noting that the time derivative Φ' entering in $\Delta_{\ell}^{\text{G3}_i}$ can usually be obtained analytically from perturbation equations, so it does not represent a numerical issue. Furthermore, when integrating by parts, to keep track of the terms representing local potential contributions, Shapiro time-delay and ISW, we introduced (inspired by [105]) the coefficients c_{lpot} , c_{std} , and c_{isw} , respectively.

References

- [1] T. Clifton, P. G. Ferreira, A. Padilla, and C. Skordis, *Modified Gravity and Cosmology*, *Phys. Rept.* **513** (2012) 1–189, [[arXiv:1106.2476](#)].
- [2] D. H. Weinberg, M. J. Mortonson, D. J. Eisenstein, C. Hirata, A. G. Riess, and E. Rozo, *Observational Probes of Cosmic Acceleration*, *Phys. Rept.* **530** (2013) 87–255, [[arXiv:1201.2434](#)].
- [3] **Planck** Collaboration, P. A. R. Ade et al., *Planck 2015 results. XIV. Dark energy and modified gravity*, [arXiv:1502.01590](#).
- [4] K. Koyama, *Cosmological Tests of Modified Gravity*, *Rept. Prog. Phys.* **79** (2016) 046902, [[arXiv:1504.04623](#)].
- [5] **Euclid** Collaboration, R. Laureijs, J. Amiaux, S. Arduini, J.-L. Augueres, J. Brinchmann, et al., *Euclid Definition Study Report*, [arXiv:1110.3193](#).
- [6] **SKA Cosmology SWG** Collaboration, R. Maartens, F. B. Abdalla, M. Jarvis, and M. G. Santos, *Overview of Cosmology with the SKA*, *PoS AASKA14* (2015) 016, [[arXiv:1501.04076](#)].

- [7] **LSST Science, LSST Project** Collaboration, P. A. Abell et al., *LSST Science Book, Version 2.0*, [arXiv:0912.0201](#).
- [8] J. Yoo, A. L. Fitzpatrick, and M. Zaldarriaga, *A New Perspective on Galaxy Clustering as a Cosmological Probe: General Relativistic Effects*, *Phys. Rev.* **D80** (2009) 083514, [[arXiv:0907.0707](#)].
- [9] C. Bonvin and R. Durrer, *What galaxy surveys really measure*, *Phys. Rev.* **D84** (2011) 063505, [[arXiv:1105.5280](#)].
- [10] A. Challinor and A. Lewis, *The linear power spectrum of observed source number counts*, *Phys. Rev.* **D84** (2011) 043516, [[arXiv:1105.5292](#)].
- [11] C. Bonvin, L. Hui, and E. Gaztanaga, *Asymmetric galaxy correlation functions*, *Phys. Rev.* **D89** (2014), no. 8 083535, [[arXiv:1309.1321](#)].
- [12] V. Iršič, E. Di Dio, and M. Viel, *Relativistic effects in Lyman- forest*, *JCAP* **1602** (2016), no. 02 051, [[arXiv:1510.03436](#)].
- [13] F. Montanari and R. Durrer, *Measuring the lensing potential with tomographic galaxy number counts*, *JCAP* **1510** (2015), no. 10 070, [[arXiv:1506.01369](#)].
- [14] D. Alonso and P. G. Ferreira, *Constraining ultralarge-scale cosmology with multiple tracers in optical and radio surveys*, *Phys. Rev.* **D92** (2015), no. 6 063525, [[arXiv:1507.03550](#)].
- [15] J. Fonseca, S. Camera, M. Santos, and R. Maartens, *Hunting down horizon-scale effects with multi-wavelength surveys*, *Astrophys. J.* **812** (2015), no. 2 L22, [[arXiv:1507.04605](#)].
- [16] W. Cardona, R. Durrer, M. Kunz, and F. Montanari, *Lensing convergence in galaxy redshift surveys*, [arXiv:1603.06481](#).
- [17] A. Joyce, B. Jain, J. Khoury, and M. Trodden, *Beyond the Cosmological Standard Model*, *Phys. Rept.* **568** (2015) 1–98, [[arXiv:1407.0059](#)].
- [18] **DESI** Collaboration, M. Levi et al., *The DESI Experiment, a whitepaper for Snowmass 2013*, [arXiv:1308.0847](#).
- [19] E. Di Dio, F. Montanari, R. Durrer, and J. Lesgourgues, *Cosmological Parameter Estimation with Large Scale Structure Observations*, *JCAP* **1401** (2014) 042, [[arXiv:1308.6186](#)].
- [20] S. Boughn and R. Crittenden, *A Correlation of the cosmic microwave sky with large scale structure*, *Nature* **427** (2004) 45–47, [[astro-ph/0305001](#)].
- [21] **Planck** Collaboration, P. A. R. Ade et al., *Planck 2013 results. XIX. The integrated Sachs-Wolfe effect*, *Astron. Astrophys.* **571** (2014) A19, [[arXiv:1303.5079](#)].
- [22] S. Ho, C. Hirata, N. Padmanabhan, U. Seljak, and N. Bahcall, *Correlation of CMB with large-scale structure: I. ISW Tomography and Cosmological Implications*, *Phys. Rev.* **D78** (2008) 043519, [[arXiv:0801.0642](#)].
- [23] T. Giannantonio, R. Crittenden, R. Nichol, and A. J. Ross, *The significance of the integrated Sachs-Wolfe effect revisited*, *Mon. Not. Roy. Astron. Soc.* **426** (2012) 2581–2599, [[arXiv:1209.2125](#)].
- [24] S. Ferraro, B. D. Sherwin, and D. N. Spergel, *WISE measurement of the integrated Sachs-Wolfe effect*, *Phys. Rev.* **D91** (2015), no. 8 083533, [[arXiv:1401.1193](#)].
- [25] Majerotto, Elisabetta and Sapone, Domenico and Schäfer, Björn Malte, *Combined constraints on deviations of dark energy from an ideal fluid from Euclid and Planck*, *Mon. Not. Roy. Astron. Soc.* **456** (2016), no. 1 109–118, [[arXiv:1506.04609](#)].
- [26] Y.-S. Song, W. Hu, and I. Sawicki, *Large scale structure of $f(r)$ gravity*, *Phys. Rev. D* **75** (Feb, 2007) 044004.

- [27] P. Zhang, *Testing gravity against the early time integrated Sachs-Wolfe effect*, *Phys. Rev. D* **73** (Jun, 2006) 123504.
- [28] J. Enander, Y. Akrami, E. Mörtzell, M. Renneby, and A. R. Solomon, *Integrated Sachs-Wolfe effect in massive bigravity*, *Phys. Rev. D* **91** (Apr, 2015) 084046.
- [29] A. Barreira, B. Li, C. Baugh, and S. Pascoli, *The observational status of Galileon gravity after Planck*, *JCAP* **1408** (2014) 059, [[arXiv:1406.0485](#)].
- [30] E. L. Wright et al., *The Wide-field Infrared Survey Explorer (WISE): Mission Description and Initial On-orbit Performance*, *Astron. J.* **140** (2010) 1868, [[arXiv:1008.0031](#)].
- [31] A. De Felice, T. Kobayashi, and S. Tsujikawa, *Effective gravitational couplings for cosmological perturbations in the most general scalar-tensor theories with second-order field equations*, *Phys. Lett.* **B706** (2011) 123–133, [[arXiv:1108.4242](#)].
- [32] L. Amendola, M. Kunz, M. Motta, I. D. Saltas, and I. Sawicki, *Observables and unobservables in dark energy cosmologies*, *Phys. Rev.* **D87** (2013), no. 2 023501, [[arXiv:1210.0439](#)].
- [33] I. Sawicki and E. Bellini, *Limits of quasistatic approximation in modified-gravity cosmologies*, *Phys. Rev.* **D92** (2015), no. 8 084061, [[arXiv:1503.06831](#)].
- [34] G. Gubitosi, F. Piazza, and F. Vernizzi, *The Effective Field Theory of Dark Energy*, *JCAP* **1302** (2013) 032, [[arXiv:1210.0201](#)]. [[JCAP1302,032\(2013\)](#)].
- [35] J. K. Bloomfield, . . Flanagan, M. Park, and S. Watson, *Dark energy or modified gravity? An effective field theory approach*, *JCAP* **1308** (2013) 010, [[arXiv:1211.7054](#)].
- [36] J. Gleyzes, D. Langlois, and F. Vernizzi, *A unifying description of dark energy*, *Int. J. Mod. Phys.* **D23** (2015), no. 13 1443010, [[arXiv:1411.3712](#)].
- [37] E. Bellini and I. Sawicki, *Maximal freedom at minimum cost: linear large-scale structure in general modifications of gravity*, *JCAP* **1407** (2014) 050, [[arXiv:1404.3713](#)].
- [38] M. Zumalacarregui, E. Bellini, I. Sawicki, and J. Lesgourgues, *Hi-CLASS: Horndeski in the Cosmic Linear Anisotropy Solving System*, [arXiv:160x.xxxxx](#). [www.hiclass-code.net](#).
- [39] L. Lombriser, J. Yoo, and K. Koyama, *Relativistic effects in galaxy clustering in a parametrized post-Friedmann universe*, *Phys. Rev.* **D87** (2013) 104019, [[arXiv:1301.3132](#)].
- [40] T. Baker and P. Bull, *Observational signatures of modified gravity on ultra-large scales*, *Astrophys. J.* **811** (2015) 116, [[arXiv:1506.00641](#)].
- [41] C.-P. Ma and E. Bertschinger, *Cosmological perturbation theory in the synchronous and conformal Newtonian gauges*, *Astrophys. J.* **455** (1995) 7–25, [[astro-ph/9506072](#)].
- [42] R. Durrer, *The Cosmic Microwave Background*. Cambridge University Press, 2008.
- [43] J. Yoo, *General Relativistic Description of the Observed Galaxy Power Spectrum: Do We Understand What We Measure?*, *Phys. Rev.* **D82** (2010) 083508, [[arXiv:1009.3021](#)].
- [44] D. Jeong, F. Schmidt, and C. M. Hirata, *Large-scale clustering of galaxies in general relativity*, *Phys. Rev.* **D85** (2012) 023504, [[arXiv:1107.5427](#)].
- [45] D. Jeong and F. Schmidt, *Large-Scale Structure with Gravitational Waves I: Galaxy Clustering*, *Phys. Rev.* **D86** (2012) 083512, [[arXiv:1205.1512](#)].
- [46] D. Wands and A. Slosar, *Scale-dependent bias from primordial non-Gaussianity in general relativity*, *Phys. Rev.* **D79** (2009) 123507, [[arXiv:0902.1084](#)].
- [47] D. Bertacca, N. Bartolo, M. Bruni, K. Koyama, R. Maartens, S. Matarrese, M. Sasaki, and D. Wands, *Galaxy bias and gauges at second order in General Relativity*, *Class. Quant. Grav.* **32** (2015), no. 17 175019, [[arXiv:1501.03163](#)].
- [48] C. Bonvin, *Isolating relativistic effects in large-scale structure*, *Class. Quant. Grav.* **31** (2014), no. 23 234002, [[arXiv:1409.2224](#)].

- [49] J. Yoo, *Relativistic Effect in Galaxy Clustering*, *Class. Quant. Grav.* **31** (2014) 234001, [[arXiv:1409.3223](#)].
- [50] L. Hui, A. Nicolis, and C. Stubbs, *Equivalence Principle Implications of Modified Gravity Models*, *Phys.Rev.* **D80** (2009) 104002, [[arXiv:0905.2966](#)].
- [51] J. Khoury and A. Weltman, *Chameleon fields: Awaiting surprises for tests of gravity in space*, *Phys.Rev.Lett.* **93** (2004) 171104.
- [52] K. Hinterbichler and J. Khoury, *Symmetron Fields: Screening Long-Range Forces Through Local Symmetry Restoration*, *Phys.Rev.Lett.* **104** (2010) 231301, [[arXiv:1001.4525](#)].
- [53] A. Vainshtein, *To the problem of nonvanishing gravitation mass*, *Phys.Lett.* **B39** (1972) 393–394.
- [54] A. Raccanelli, D. Bertacca, D. Jeong, M. C. Neyrinck, and A. S. Szalay, *Doppler term in the galaxy two-point correlation function: wide-angle, velocity, Doppler lensing and cosmic acceleration effects*, [arXiv:1602.03186](#).
- [55] U. Seljak, *Extracting primordial non-gaussianity without cosmic variance*, *Phys. Rev. Lett.* **102** (2009) 021302, [[arXiv:0807.1770](#)].
- [56] C. Bonvin, L. Hui, and E. Gaztanaga, *Optimising the measurement of relativistic distortions in large-scale structure*, [arXiv:1512.03566](#).
- [57] E. Gaztanaga, C. Bonvin, and L. Hui, *Measurement of the dipole in the cross-correlation function of galaxies*, [arXiv:1512.03918](#).
- [58] A. Raccanelli, D. Bertacca, O. Doré, and R. Maartens, *Large-scale 3D galaxy correlation function and non-Gaussianity*, *JCAP* **1408** (2014) 022, [[arXiv:1306.6646](#)].
- [59] G. W. Horndeski, *Second-order scalar-tensor field equations in a four-dimensional space*, *Int. J. Theor. Phys.* **10** (1974) 363–384.
- [60] R. P. Woodard, *Ostrogradsky’s theorem on Hamiltonian instability*, *Scholarpedia* **10** (2015), no. 8 32243, [[arXiv:1506.02210](#)].
- [61] M. Zumalacarregui and J. Garcia-Bellido, *Transforming gravity: from derivative couplings to matter to second-order scalar-tensor theories beyond the Horndeski Lagrangian*, *Phys.Rev.* **D89** (2014) 064046, [[arXiv:1308.4685](#)].
- [62] J. Gleyzes, D. Langlois, F. Piazza, and F. Vernizzi, *Healthy theories beyond Horndeski*, *Phys. Rev. Lett.* **114** (2015), no. 21 211101, [[arXiv:1404.6495](#)].
- [63] T. Kobayashi, Y. Watanabe, and D. Yamauchi, *Breaking of Vainshtein screening in scalar-tensor theories beyond Horndeski*, *Phys. Rev.* **D91** (2015), no. 6 064013, [[arXiv:1411.4130](#)].
- [64] D. Pirtskhalava, L. Santoni, E. Trinchieri, and F. Vernizzi, *Weakly Broken Galileon Symmetry*, *JCAP* **1509** (2015), no. 09 007, [[arXiv:1505.00007](#)].
- [65] M. Crisostomi, M. Hull, K. Koyama, and G. Tasinato, *Horndeski: beyond, or not beyond?*, *JCAP* **1603** (2016), no. 03 038, [[arXiv:1601.04658](#)].
- [66] C. Brans and R. Dicke, *Mach’s principle and a relativistic theory of gravitation*, *Phys.Rev.* **124** (1961) 925–935.
- [67] C. Deffayet, O. Pujolas, I. Sawicki, and A. Vikman, *Imperfect Dark Energy from Kinetic Gravity Braiding*, *JCAP* **1010** (2010) 026, [[arXiv:1008.0048](#)].
- [68] C. Deffayet, G. Esposito-Farese, and A. Vikman, *Covariant Galileon*, *Phys.Rev.* **D79** (2009) 084003, [[arXiv:0901.1314](#)].

- [69] C. Deffayet, S. Deser, and G. Esposito-Farese, *Generalized Galileons: All scalar models whose curved background extensions maintain second-order field equations and stress-tensors*, *Phys.Rev.* **D80** (2009) 064015, [[arXiv:0906.1967](#)].
- [70] A. Maselli, H. O. Silva, M. Minamitsuji, and E. Berti, *Slowly rotating black hole solutions in Horndeski gravity*, *Phys. Rev.* **D92** (2015), no. 10 104049, [[arXiv:1508.03044](#)].
- [71] J. M. Ezquiaga, J. García-Bellido, and M. Zumalacárregui, *Towards the most general scalar-tensor theories of gravity: a unified approach in the language of differential form*, [arXiv:1603.01269](#).
- [72] M. Zumalacarregui, T. S. Koivisto, and D. F. Mota, *DBI Galileons in the Einstein Frame: Local Gravity and Cosmology*, *Phys. Rev.* **D87** (2013) 083010, [[arXiv:1210.8016](#)].
- [73] D. Bettoni and S. Liberati, *Disformal invariance of second order tensor-scalar theories: framing the Horndeski action*, *Phys.Rev.* **D88** (2013) 084020, [[arXiv:1306.6724](#)].
- [74] C. Charmousis, E. J. Copeland, A. Padilla, and P. M. Saffin, *General second order scalar-tensor theory, self tuning, and the Fab Four*, *Phys.Rev.Lett.* **108** (2012) 051101, [[arXiv:1106.2000](#)].
- [75] P. Martin-Moruno, N. J. Nunes, and F. S. N. Lobo, *Horndeski theories self-tuning to a de Sitter vacuum*, *Phys. Rev.* **D91** (2015), no. 8 084029, [[arXiv:1502.03236](#)].
- [76] J. Gleyzes, D. Langlois, F. Piazza, and F. Vernizzi, *Essential Building Blocks of Dark Energy*, *JCAP* **1308** (2013) 025, [[arXiv:1304.4840](#)].
- [77] E. Bellini, R. Jimenez, and L. Verde, *Signatures of Horndeski gravity on the Dark Matter Bispectrum*, *JCAP* **1505** (2015), no. 05 057, [[arXiv:1504.04341](#)].
- [78] E. Bellini and M. Zumalacarregui, *Nonlinear evolution of the baryon acoustic oscillation scale in alternative theories of gravity*, *Phys. Rev.* **D92** (2015), no. 6 063522, [[arXiv:1505.03839](#)].
- [79] D. Bettoni and M. Zumalacrregui, *Shaken, not Stirred: Kinetic mixing in scalar-tensor theories of gravity*, *Phys. Rev.* **D91** (2015) 104009, [[arXiv:1502.02666](#)].
- [80] I. D. Saltas, I. Sawicki, L. Amendola, and M. Kunz, *Anisotropic Stress as a Signature of Nonstandard Propagation of Gravitational Waves*, *Phys. Rev. Lett.* **113** (2014), no. 19 191101, [[arXiv:1406.7139](#)].
- [81] A. Nicolis, R. Rattazzi, and E. Trincherini, *The Galileon as a local modification of gravity*, *Phys. Rev.* **D79** (2009) 064036, [[arXiv:0811.2197](#)].
- [82] A. Barreira, B. Li, C. Baugh, and S. Pascoli, *Linear perturbations in Galileon gravity models*, [arXiv:1208.0600](#).
- [83] A. Barreira, B. Li, A. Sanchez, C. M. Baugh, and S. Pascoli, *The parameter space in Galileon gravity models*, *Phys.Rev.* **D87** (2013) 103511, [[arXiv:1302.6241](#)].
- [84] S. A. Appleby and E. V. Linder, *Trial of Galileon gravity by cosmological expansion and growth observations*, *JCAP* **1208** (2012) 026, [[arXiv:1204.4314](#)].
- [85] A. Barreira, B. Li, W. A. Hellwing, C. M. Baugh, and S. Pascoli, *Nonlinear structure formation in the Cubic Galileon gravity model*, *JCAP* **1310** (2013) 027, [[arXiv:1306.3219](#)].
- [86] B. Li, A. Barreira, C. M. Baugh, W. A. Hellwing, K. Koyama, S. Pascoli, and G.-B. Zhao, *Simulating the quartic Galileon gravity model on adaptively refined meshes*, *JCAP* **1311** (2013) 012, [[arXiv:1308.3491](#)].
- [87] E. Bellini, A. J. Cuesta, R. Jimenez, and L. Verde, *Constraints on deviations from Λ CDM within Horndeski gravity*, [arXiv:1509.07816](#).
- [88] E. Mörtzell and J. Enander, *Scalar instabilities in bimetric gravity: The Vainshtein mechanism and structure formation*, *JCAP* **1510** (2015), no. 10 044, [[arXiv:1506.04977](#)].

- [89] F. König, *Higuchi Ghosts and Gradient Instabilities in Bimetric Gravity*, *Phys. Rev.* **D91** (2015) 104019, [[arXiv:1503.07436](#)].
- [90] A. Barreira, B. Li, C. Baugh, and S. Pascoli, *Modified gravity with massive neutrinos as a testable alternative cosmological model*, *Phys. Rev.* **D90** (2014), no. 2 023528, [[arXiv:1404.1365](#)].
- [91] **Planck** Collaboration, P. A. R. Ade et al., *Planck 2015 results. XIII. Cosmological parameters*, [arXiv:1502.01589](#).
- [92] A. Raccanelli, D. Bertacca, R. Maartens, C. Clarkson, and O. Doré, *Lensing and time-delay contributions to galaxy correlations*, [arXiv:1311.6813](#).
- [93] E. Aubourg et al., *Cosmological implications of baryon acoustic oscillation measurements*, *Phys. Rev.* **D92** (2015), no. 12 123516, [[arXiv:1411.1074](#)].
- [94] **BOSS** Collaboration, A. Font-Ribera et al., *Quasar-Lyman α Forest Cross-Correlation from BOSS DR11 : Baryon Acoustic Oscillations*, *JCAP* **1405** (2014) 027, [[arXiv:1311.1767](#)].
- [95] **BOSS** Collaboration, T. Delubac et al., *Baryon acoustic oscillations in the Ly forest of BOSS DR11 quasars*, *Astron. Astrophys.* **574** (2015) A59, [[arXiv:1404.1801](#)].
- [96] **Planck Collaboration** Collaboration, P. Ade et al., *Planck 2013 results. XVI. Cosmological parameters*, [arXiv:1303.5076](#).
- [97] R. K. Sachs and A. M. Wolfe, *Perturbations of a cosmological model and angular variations of the microwave background*, *Astrophys. J.* **147** (1967) 73–90. [Gen. Rel. Grav.39,1929(2007)].
- [98] T. Lu, U.-L. Pen, and O. Doré, *Dark Energy from Large-Scale Structure Lensing Information*, *Phys. Rev.* **D81** (2010) 123015, [[arXiv:0905.0499](#)].
- [99] K. W. Masui, F. Schmidt, U.-L. Pen, and P. McDonald, *Projected Constraints on Modified Gravity Cosmologies from 21cm Intensity Mapping*, *Phys. Rev.* **D81** (2010) 062001, [[arXiv:0911.3552](#)].
- [100] A. R. Pullen, S. Alam, S. He, and S. Ho, *Constraining Gravity at the Largest Scales through CMB Lensing and Galaxy Velocities*, [arXiv:1511.04457](#).
- [101] L. Lombriser and A. Taylor, *Semi-dynamical perturbations of unified dark energy*, *JCAP* **1511** (2015), no. 11 040, [[arXiv:1505.05915](#)].
- [102] N. Kaloper, A. Padilla, D. Stefanyszyn, and G. Zahariade, *Manifestly Local Theory of Vacuum Energy Sequestering*, *Phys. Rev. Lett.* **116** (2016), no. 5 051302, [[arXiv:1505.01492](#)].
- [103] D. Blas, J. Lesgourgues, and T. Tram, *The Cosmic Linear Anisotropy Solving System (CLASS) II: Approximation schemes*, *JCAP* **1107** (2011) 034, [[arXiv:1104.2933](#)].
- [104] E. Di Dio, F. Montanari, J. Lesgourgues, and R. Durrer, *The CLASSgal code for Relativistic Cosmological Large Scale Structure*, *JCAP* **1311** (2013) 044, [[arXiv:1307.1459](#)].
- [105] J. Lesgourgues and T. Tram, *Fast and accurate CMB computations in non-flat FLRW universes*, *JCAP* **1409** (2014), no. 09 032, [[arXiv:1312.2697](#)].